ORCA – Online Research @ Cardiff

Guaranteed error bounds in homogenisation: an optimum stochastic approach to preserve the numerical separation of scales

D. A. Paladim [*1], J. P. Moitinho de Almeida[2], S. P. A. Bordas[1,3], and P. Kerfriden[†1]

[1]Cardiff School of Engineering
[2]Instituto Superior Técnico, University of Lisbon
[3]Université du Luxembourg

Abstract

This paper proposes a new methodology to guarantee the accuracy of the homogenisation schemes that are traditionally employed to approximate the solution of PDEs with random, fast evolving diffusion coefficients. We typically consider linear elliptic diffusion problems in randomly packed particulate composites. Our work extends the pioneering work presented in [26, 32] in order to bound the error in the expectation and second moment of quantities of interest, without ever solving the fine-scale, intractable stochastic problem. The most attractive feature of our approach is that the error bounds are computed without any integration of the fine-scale features. Our computations are purely macroscopic, deterministic, and remain tractable even for small scale ratios. The second contribution of the paper is an alternative derivation of modelling error bounds through the Prager-Synge hypercircle theorem. We show that this approach allows us to fully characterise and optimally tighten the interval in which predicted quantities of interest are guaranteed to lie. We interpret our optimum result as an extension of Reuss-Voigt approaches, which are classically used to estimate the homogenised diffusion coefficients of composites, to the estimation of macroscopic engineering quantities of interest. Finally, we make use of these derivations to obtain an efficient procedure for multiscale model verification and adaptation.

1   Introduction

Composites play an increasing role in modern mechanical systems. This raises tremendous challenges for computational mechanics. Indeed, the direct modelling of such systems results in intractable problems due to the fast spatial variations of material properties. The analysis of realistic composite systems requires an additional modelling step, whereby the microscopic constituents are substituted by a single material in such a way that this resulting model captures the global behaviour of the system. This process is known as homogenisation (see for example [22, 38]). The theory of homogenisation is well

---

[*]Contact e-mail: AlvesPaladimD@cardiff.ac.uk
[†]Contact e-mail: pierre.kerfriden@gmail.com

established for linear elliptic operators. In particular, homogenisation can be seen as the limit of heterogeneous problems when the scale ratio tends to zero [34]. However, most composite systems used in engineering exhibit a weak scale separation. Worse still, the most interesting features of mechanical problems are located in regions where the scale separation is lost altogether, typically in regions of steep gradients (*e.g.* stress concentration in solid mechanics, localised limit-states such as damage, sharp geometrical irregularities, *etc.*). In such cases, the results provided by homogenised schemes may differ significantly from the results that would be obtained by solving the fine-scale problem directly. There is a strong need to quantify this discrepancy, and derive efficient algorithms to keep it under control, in order to ensure that the simulation of physical processes over multiple scales remains predictive.
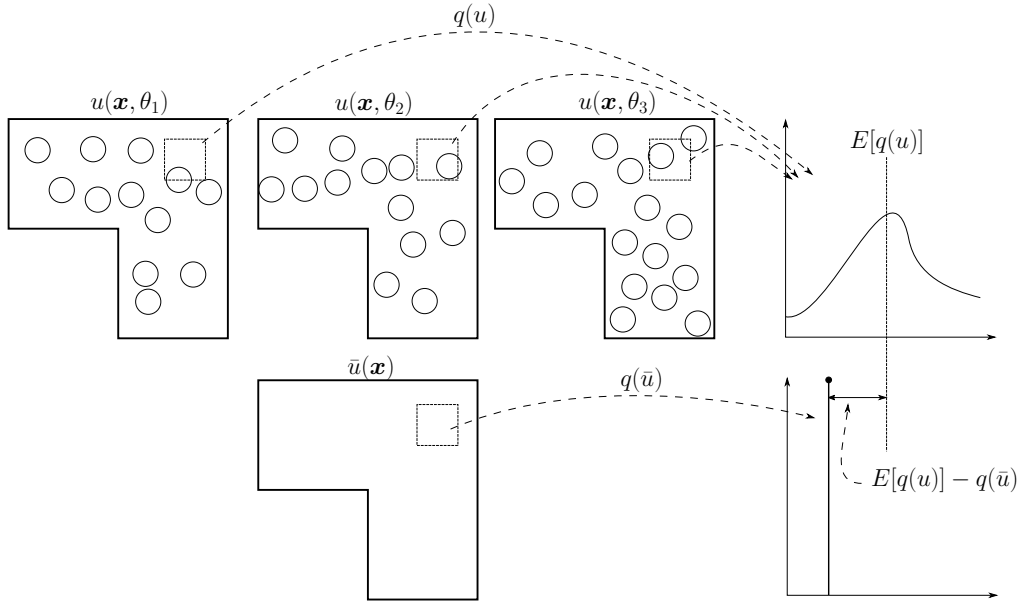

Figure 1: In the framework presented in this paper, the accuracy of homogenisation, $\bar{u}$, is measured in terms of the "true" intractable stochastic model u. Direct approximation of a quantities of interest, $q(u)$, a random variable, is not possible. Instead, we estimate $q(\bar{u})$ (a deterministic quantity) and bound the statistical moments of the difference, $q(u) - q(\bar{u})$.

Estimating and controlling errors arising from the homogenisation of microscopically heterogeneous structures remains a relatively immature research field compared to that of controlling errors due to traditional discretisation schemes (see *e.g.* [2, 6, 8, 16, 35] for a good account of the state-of-the art of *a posteriori* error estimation the context of the Finite Element Method). Over the last two decades, researchers have attempted to derive heuristic criteria to indicate regions of computational domains where multiscale models fail to be predictive. In these regions, the macroscopic model is typically bypassed and replaced by the microscopic one. Such adaptive approaches typically rely on error indicators based on internal variables such as damage indicators, or based on local measures of the steepness of macroscopic gradients. Unfortunately, these heuristics do not provide a quantitative measure of modelling errors, and are usually highly problem-sensitive. However, the rationale underlying the use of "gradients of gradients" as a local error indicator of homogenisation schemes is relatively clear: higher order terms of homogenisation expansions can be computed in order to serve as an

approximation of the difference between the solution of the multiscale surrogate and that of the intractable microscopic solution. Recent contributions to this topic can be found in [3, 17, 18, 30, 36, 37]. The last two of these publications rely on a stronger mathematical basis linking verification methodologies based on enhanced homogenisation schemes and well-established residual-based error estimation frameworks. Although such schemes are not fully developed nor exhaustively tested, these developments show that the trend is to move from qualitative upscaling error estimation towards the quantification of the accuracy of multiscale approximations.

In the last decade, a restricted number of research groups have attempted to *guarantee* the accuracy of multiscale approximations through the application of rigorous *a posteriori* numerical error analysis techniques. In this new area, the contributions that have inspired us most are that of A. Abdulle's group [1] and that of the J.T. Oden's group. In a series of papers [20, 23–26, 32, 33, 39, 42], the latter group was able to develop constant-free error bounds on certain measures of multiscale modelling errors, namely the "energy norm" of the error and the error in linear engineering quantities of interest (through the application of the adjoint methodology [5, 25]). Using these bounds, model adaptivity can be performed by replacing the surrogate macroscale model by its underlying microscale counterpart in the regions where the local contribution to the error bound is large. However, this modelling error bounding technique suffers from certain limitations, the most important of which is the fact that the bounds require the computation of terms involving the fine-scale description of the material properties. In practice, this means that the fine-scale heterogeneities need to be meshed, which becomes quickly intractable as the scale ratio increases. Secondly, the error is not strictly bounded, and a *sufficiently fine* macroscopic mesh needs to be used for the bounding properties to hold in practical applications. Finally, the various parameters that affect the quality of the error bounds, not the least of which is the type of homogenised model that is used to obtain an approximate solution to the fine-scale problem, are difficult to characterise and fully optimise.

The work presented in this paper builds on these pioneering investigations and addresses some of the key limitations of available multiscale modelling error bounding technology. Our fundamental suggestion is to allow for the position of the heterogeneities to be governed by a random process. In this setting, we aim to estimate (a) the expectation of "energy-norm" and of "goal-oriented" measures of the error (*i.e.* statistical average) and (b) the moments of these measures (*i.e.* statistical dispersion). In addition to being a realistic modelling setting for heterogeneous media, the direct consequence of this choice is that the computation of the error bounds only involves an integral of a function that, under weakly restrictive assumptions, varies slowly in space. This allows the application of upscaling error bounding without any restriction in terms of scale ratio. As it can be seen in fig. 1, the problem of error estimation is interpreted in terms of two models, a stochastic intractable model ("true" model) which includes the microscale, and a tractable surrogate homogenised model. We aim to charaterise the former by studying the latter.

At this point, it is important to acknowledge that our approach to modelling error bounding is closely related to the area of spectral stochastic finite element methods. Those methods seek to approach the response surface of the system by discretising the random field using a Karhunen-Loève expansion and by representing the nodal unknowns using polynomial chaos [10](see also [4, 19]). However, those methods do not apply to the present problem. A parametrization of the random field is not readily available and though it can be obtained, its Karhunen-Loève expansion converges very slowly to it.

Our second contribution is the development of a general error bounding framework in which the efficiency of the error estimates can be fully characterised and controlled. In order to achieve this difficult task, we propose to base our bounding approach on

the Prager-Synge hypercircle theorem [27]. The resulting error bounds are strictly guaranteed and the "true" model is approximated by a pair of surrogates generated from different homogenisation schemes associated with complementary discretisation techniques (namely the compatible and the admissible FEM), instead of single field as proposed in [26]. This pair exhibits very strong similarities to those used to derive the classical Reuss-Voigt bounds for effective medium properties. Such an interesting property will give us a very strong background to characterise, both intuitively and mathematically, and to fully optimise the efficiency of the error estimates (*i.e.* minimise the remaining uncertainty on predicted quantities).

Once this new framework has been established, we proceed as in [32] and show that more accurate and guaranteed estimates can be obtained through locally replacing the homogenised surrogates by the "true" microscopic model. We call *adaptive modelling* this dynamic, hybrid approximation with elements of the "true" and surrogate model working together towards the accurate bounding of engineering quantities of interest. New local error indicators will also be presented to guide this adaptive modelling process.

The paper is organised as follows. In section 2, we introduce the problem of multiscale error estimation. In section 3, we present both lower and upper bounds for the error in energy norm and error in quantities of interest. We conclude this section by describing the strategy that we will use to adapt our multiscale modelling. Finally, we present numerical examples in section 4.

2 Problem formulation

2.1 Reference ("true") model

We consider the problem of stationary heat conduction in a body Ω defined in a subset of $\mathbb{R}^d$ ($d = 1, 2, 3$). The boundary of this domain is denoted by Γ and can be further divided in two parts Γ_N and Γ_D, Neumann and Dirichlet boundary, such that $\Gamma_D \neq \emptyset$, $\Gamma_D \cup \Gamma_N = \Gamma$ and $\Gamma_D \cap \Gamma_N = \emptyset$. Deterministic fluxes g are prescribed on Γ_N, deterministic temperatures h are prescribed on Γ_D and a deterministic source term f that accounts for the internal heat generation is applied over the interior of the domain. The different phases in the domain are distributed according to a random process. We target applications such as modelling random particulate composites (e.g. concrete) or heterogeneous media with a random distribution of polygonal phases (e.g. idealised microstructure of a metallic phase) that can be generated by Poisson point process and a rejection rule. The resulting conductivity k is a function of the spatial domain Ω and the stochastic domain Θ, that accounts for all the possible heterogeneities layouts. It is assumed that the expectation of the conductivity $E[k](\boldsymbol{x})$ and of its reciprocal $E[k^{-1}](\boldsymbol{x})$ are known for all $\boldsymbol{x} \in \Omega$.

The random heat conduction problem for the temperature field u reads:

For each $\theta \in \Theta$ and for all $v(\boldsymbol{x}) \in \mathcal{U}_0$, find $u(\boldsymbol{x}, \theta) \in \mathcal{U}$

$$\int_{\Omega} k(\boldsymbol{x}, \theta) \, \nabla u(\boldsymbol{x}, \theta) \cdot \nabla v(\boldsymbol{x}) \, d\Omega = \int_{\Omega} f(\boldsymbol{x}) v(\boldsymbol{x}) \, d\Omega - \int_{\Gamma_N} g(\boldsymbol{x}) v(\boldsymbol{x}) \, d\Gamma \qquad (1)$$

where

$$\mathcal{U} = \{u \in H^1(\Omega) : u(\boldsymbol{x}) = h(\boldsymbol{x}) \quad \forall \boldsymbol{x} \in \Gamma_D\}$$
$$\mathcal{U}_0 = \{u \in H^1(\Omega) : u(\boldsymbol{x}) = 0 \quad \forall \boldsymbol{x} \in \Gamma_D\}.$$

and $H^1(\Omega)$ is the Sobolev space of square integrable functions with square integrable first derivatives on Ω. The elements of $\mathcal{U}$ are called kinematically admissible (KA) following the nomenclature of [15]. The left hand side of eq. (1) is a positive (semi-) definite bilinear form that will be denoted by

$$a_\theta(u,v) = \int_\Omega k(\boldsymbol{x}, \theta) \nabla u(\boldsymbol{x}) \cdot \nabla v(\boldsymbol{x}) \, d\Omega$$

while its induced (semi-) norm will be denoted by

$$\|v\|_\theta = \sqrt{a_\theta(v,v)}.$$

The right hand side of eq. (1) is a linear form that will be denoted by

$$l(v) = \int_\Omega f(\boldsymbol{x})v(\boldsymbol{x})d\Omega - \int_{\Gamma_N} v(\boldsymbol{x})g(\boldsymbol{x})d\Gamma.$$

2.2 Homogenisation surrogate

Our aim is to solve the problem in eq. (1) approximately when the random conductivity field exhibits fast spatial variations. In this context, traditional homogenisation approaches seek to define a set of deterministic governing equations that produces a good approximation of the expectation of u, the random solution field of the reference problem in eq. (1). Such an homogenisation problem typically involves replacing the random diffusion coefficient field by an homogenised, deterministic conductivity field $\bar{k}$:

For all $v \in \mathcal{U}_0$, find $\bar{u} \in \mathcal{U}$

$$\int_\Omega \bar{k}(\boldsymbol{x}) \nabla \bar{u}(\boldsymbol{x}) \cdot \nabla v(\boldsymbol{x}) \, d\Omega = l(v). \tag{2}$$

The bilinear form of the left hand side of eq. (2) will be referred as

$$\bar{a}(u,v) := \int_\Omega \bar{k}(\boldsymbol{x}) \nabla \bar{u}(\boldsymbol{x}) \cdot \nabla v(\boldsymbol{x})d\Omega. \tag{3}$$

The spatial variations of $\bar{k}$ are typically slow. The expression of $\bar{k}$ can be obtained, for instance, by using the theory of asymptotic homogenisation of periodic media, choosing a very large unit cell as representative volume element [34] or by using analytical approximations (Mori-Tanaka diffuse estimates [21], Hashin-Strikman bounds [12],...). The homogenised problem can be solved by traditional numerical methods for deterministic boundary value problems. We will make use of the Finite Element Method (FEM). The approximate solution of the homogenised problem delivered by the FEM will be denoted by $\bar{u}^h \in \mathcal{U}^h \subseteq \mathcal{U}$.

2.3 Error field and error measures

The stochastic error field will be denoted by $e(\boldsymbol{x}, \theta) = u(\boldsymbol{x}, \theta) - \bar{u}^h(\boldsymbol{x})$. For the sake of clarity, we will use the same notation for the solution of the homogenised problem, and its deterministic prolongation into the space of random temperature fields, $\bar{u}$. This error is due to two interacting sources of approximation: (i) the finite element discretisation

of the homogenised problem and (ii) the approximation of the reference problem by an homogenised surrogate. This can be expressed mathematically as:

$$e = (u - \bar{u}) + (\bar{u} - \bar{u}^h) = e^{\mathrm{H}} + e^{\mathrm{d}} \tag{4}$$

where e^{d} is the error of discretisation, e^{H} the error of homogenisation, and $\bar{u}$ is the intractable solution to the exact homogenisation problem eq. (2) (without FEM).

To introduce the necessary notations, we note that the error field is governed by the stochastic problem

$$a_\theta(e, v) = R_\theta(v) \quad \forall v \in \mathcal{U}_0 \tag{5}$$

where the residual is a linear form defined as

$$R_\theta(v) := l(v) - a_\theta(\bar{u}^h, v). \tag{6}$$

Solving for e is a problem as intractable as solving for the intractable reference solution u. A more tractable goal is to estimate bounds for the norm of this field. The work of [26] could be applied to obtain bounds for each realisation independently; however, as already mentioned in the introduction, this would still involve the generation of an integration mesh for each of the realisations. For this reason, we aim to obtain bounds for

$$\|e\| := \sqrt{a(e, e)}$$

where

$$a(u, v) = E[a_\theta(u, v)] \quad \text{with } u, v \in \mathcal{U}_\theta,$$

and

$$\mathcal{U}_\theta = \{v \,|\, \forall \theta \in \Theta \quad v(\boldsymbol{x}, \theta) \in \mathcal{U}_0 \text{ and } \|v\| < \infty\}. \tag{7}$$

As it will be seen, the choice of this specific quantity allows us to exploit the smoothness of the expected conductivity field ($E[k](\boldsymbol{x})$) and obtain bounds that do not involve the generation of realisations and/or additional integration meshes[1].

We also aim to estimate the error in the so called quantities of interest (QoI). QoIs represent the objectives of the analysis, such as the flux through part of the boundary or the average temperature in part of the domain. Such quantities will be restricted to linear functionals q_θ applied to the solution u. Our goal is to compare $q_\theta(\bar{u}^h)$, the surrogate QoI to the true QoI. More precisely, we aim to bound the expectation and the moments of $q_\theta(u) - q_\theta(\bar{u}^h)$.

3   Guaranteed modelling error bounds

The modelling error estimation framework that we develop in this paper is based on the Prager-Synge hypercircle which requires a statically admissible (SA) field. We start by defining SA fields and describing how such fields can be computed.

3.1   Complementary formulation

The problem in eq. (2) can be also formulated in terms of fluxes [41]. This formulation is also called complementary formulation and the corresponding "true" problem reads,

For each $\theta \in \Theta$ and for all $\boldsymbol{p} \in \mathcal{S}_0$, find $\boldsymbol{q}(\boldsymbol{x}, \theta) \in \mathcal{S}$

$$\int_\Omega k^{-1}(\boldsymbol{x}, \theta)\, \boldsymbol{q}(\boldsymbol{x}, \theta) \cdot \boldsymbol{p}(\boldsymbol{x})\, d\Omega = \int_{\Gamma_D} \boldsymbol{p}(\boldsymbol{x}) \cdot \boldsymbol{n}(\boldsymbol{x})\, h(\boldsymbol{x})\, d\Gamma \tag{8}$$

---

[1] See section 3.2.1 for a discussion on bounding the quantity $E[\|e\|_\theta]$

where

$$\mathcal{S} = \{\boldsymbol{q} \in H^{\mathrm{div}}(\Omega) \, : \, \boldsymbol{q}(\boldsymbol{x}) \cdot n(\boldsymbol{x}) = g(\boldsymbol{x}) \quad \forall \boldsymbol{x} \in \Gamma_N \text{ and } \nabla \cdot \boldsymbol{q}(\boldsymbol{x}) = f(\boldsymbol{x}) \qquad \forall \boldsymbol{x} \in \Omega\},$$

$$\mathcal{S}_0 = \{\boldsymbol{q} \in H^{\mathrm{div}}(\Omega) \, : \, \boldsymbol{q}(\boldsymbol{x}) \cdot n(\boldsymbol{x}) = 0 \qquad \forall \boldsymbol{x} \in \Gamma_N \text{ and } \nabla \cdot \boldsymbol{q}(\boldsymbol{x}) = 0 \qquad \forall \boldsymbol{x} \in \Omega\},$$

$H^{\mathrm{div}}(\Omega)$ is the Sobolev space of square integrable functions with square integrable divergences on Ω and $\boldsymbol{n}$ denotes the outward unit normal vector on Γ. The elements of $\mathcal{S}$ are said to be statically admissible (SA). We note that $\boldsymbol{q} = -k\nabla u$. This problem is also intractable. We also introduce the following surrogate model,

---

For all $\boldsymbol{p} \in \mathcal{S}_0$, find $\hat{\boldsymbol{q}} \in \mathcal{S}$

$$\int_{\Omega} \hat{k}^{-1}(\boldsymbol{x}) \, \hat{\boldsymbol{q}}(\boldsymbol{x}) \cdot \boldsymbol{p}(\boldsymbol{x}) \, d\Omega = \int_{\Gamma_D} \boldsymbol{p}(\boldsymbol{x}) \cdot \boldsymbol{n}(\boldsymbol{x}) \, h(\boldsymbol{x}) \, d\Gamma \tag{9}$$

---

where $\hat{k}$ is again an homogenised, deterministic conductivity field, possibly different from $\bar{k}$. We note that if $\hat{k} = \bar{k}$ then $\hat{\boldsymbol{q}} = -\bar{k}\nabla\bar{u}$.

A numerical solution $\hat{\boldsymbol{q}}^h$ of the homogenised problem is sought in the space of statically admissible fluxes by means of a hybrid equilibrium finite element formulation. This ensures that the bounds presented later on are strictly guaranteed. Details of the numerical approximation can be found in appendix A.4 and in [7].

3.2 Estimates for the error in the energy norm

3.2.1 Upper bound for the energy-norm of the error

Our aim in this section is to obtain an upper bound to the quantity $\|e\|$. We recall that for every realisation θ, the Prager-Synge hypercircle theorem [27] can be applied to u (the solution of eq. (1)) and to our approximations $\bar{u}^h$ and $\hat{\boldsymbol{q}}^h$ to obtain,

$$\|\hat{\boldsymbol{q}}^h + k\nabla\bar{u}^h\|^2_{k^{-1},\theta} = \|\mathbf{e}^q\|^2_{k^{-1},\theta} + \|e\|^2_{\theta} \tag{10}$$

where

$$\|\boldsymbol{v}\|^2_{k^{-1},\theta} = \int_{\Omega} k^{-1}(\boldsymbol{x},\theta)\boldsymbol{v}(\boldsymbol{x}) \cdot \boldsymbol{v}(\boldsymbol{x}) \, d\Omega$$
$$\mathbf{e}^q = -k\nabla u - \hat{\boldsymbol{q}}^h.$$

By taking expectations on both sides, we obtain

$$E[\|\hat{\boldsymbol{q}}^h + k\nabla\bar{u}^h\|^2_{k^{-1},\theta}] = E[\|\mathbf{e}^q\|^2_{k^{-1},\theta}] + \|e\|^2. \tag{11}$$

From the non-negativity of the terms in eq. (11), we obtain the bound

$$\|e\|^2 \le E[\|\hat{\boldsymbol{q}}^h + k\nabla\bar{u}^h\|^2_{k^{-1},\theta}] =: \eta^2 \tag{12}$$

The quantity η is usually called constitutive relation error (CRE) [14–16].

Several remarks must be made regarding this result. Firstly, by expanding η^2,

$$\eta^2 = \int_{\Omega} E[k^{-1}](\boldsymbol{x})\hat{\boldsymbol{q}}^h(\boldsymbol{x}) \cdot \hat{\boldsymbol{q}}^h(\boldsymbol{x}) \, d\Omega + \int_{\Omega} E[k](\boldsymbol{x})\nabla\bar{u}^h(\boldsymbol{x}) \cdot \nabla\bar{u}^h(\boldsymbol{x}) \, d\Omega$$
$$+ 2\int_{\Omega} \hat{\boldsymbol{q}}^h(\boldsymbol{x}) \cdot \nabla\bar{u}^h(\boldsymbol{x}) \, d\Omega \tag{13}$$

it becomes clear that the computation of the bound does not involve dealing with each of the realisations. Furthermore, as previously announced, it does not require the generation of an additional integration mesh, provided that $E[k]$ and $E[k^{-1}]$ are smooth over the domain, as opposed to the work in [20, 23–26, 32, 33, 39, 42]. Moreover, the derivation presented in the mentioned works(except for [20]) prescribes $\hat{\boldsymbol{q}}^h = -\bar{k}\bar{u}$ [2]. In general, this has a negative impact on the effectivity of the bound, since it is controlled by how well $\hat{\boldsymbol{q}}^h$ approximates the reference flux $-k\nabla u$,

$$\frac{\eta}{\|e\|} = \sqrt{\frac{\|e\|^2 + E[\|\mathbf{e}^q\|^2_{k^{-1},\theta}]}{\|e\|^2}} = \sqrt{1 + \frac{E[\|\mathbf{e}^q\|^2_{k^{-1},\theta}]}{\|e\|^2}}. \tag{14}$$

Assuming that the error in the flux field is of the same order of the error in the temperature field, an effectivity of $\sqrt{2}$ is to be expected.

Finally, we expand on the discussion started on section 2.3 regarding the quantity $E[\|e\|_\theta]]$. It can be upper bounded by taking expectations of the following inequality,

$$\|e\|_\theta \le \|\hat{\boldsymbol{q}}^h + k\bar{u}^h\|_{k^{-1},\theta}. \tag{15}$$

However, the computation of this bound would involve the generation of a integration mesh for each of the realisations. We also note the following relation between $E[\|e\|_\theta]$ and $\|e\|$, due to the definition of variance,

$$\text{Var}[\|e\|_\theta] := E[(\|e\|_\theta - E[\|e\|_\theta])^2] = \|e\|^2 - E[\|e\|_\theta]^2 \Rightarrow E[\|e\|_\theta]^2 \le \|e\|^2 \tag{16}$$

which implies that η also upper bounds $E[\|e\|_\theta]$ with effectivity

$$\frac{\eta}{E[\|e\|_\theta]} = \sqrt{1 + \frac{\text{Var}[\|e\|_\theta]}{E[\|e\|_\theta]^2} + \frac{E[\|\mathbf{e}^q\|^2_{k^{-1},\theta}]}{E[\|e\|_\theta]^2}}. \tag{17}$$

Loosely speaking, if the variance is small, we may expect that η is a practical upper bound for each of the realisations independently.

Remark 1. *Similarly, it is possible to derive bounds for $E[\|\mathbf{e}^q\|^2_{k^{-1},\theta}]$, however we will not explore this possibility in the present paper.*

3.2.2   A lower bound for the error in energy norm

We follow the steps proposed in [25] to derive a lower bound. The following identity is a direct consequence of the Cauchy-Schwarz inequality,

$$\|e\| = \sup_{v\in\mathcal{U}_\theta\backslash\{0\}} \frac{|a(e,v)|}{\|v\|}. \tag{18}$$

Combining with eq. (5),

$$\sup_{v\in\mathcal{U}_\theta\backslash\{0\}} \frac{|a(e,v)|}{\|v\|} = \sup_{v\in\mathcal{U}_\theta\backslash\{0\}} \frac{|R(v)|}{\|v\|} \ge \frac{|R(w)|}{\|w\|} \quad \forall w \in \mathcal{U}_\theta\backslash\{0\} \tag{19}$$

where

$$R(v) := E[R_\theta(v)]. \tag{20}$$

To simplify the computation of the bound, it is desirable to choose w in $\mathcal{U}_0^h$. The element in $\mathcal{U}_0^h$ that maximises the lower bound is Πe where Π is the orthogonal projection operator

---

[2]The discretisation error is neglected.

on $\mathcal{U}_0^h$ with respect to $a(\cdot, \cdot)$. Indeed, by using the defining properties of orthogonal projection and the Cauchy-Schwarz inequality, we obtain the following

$$\frac{|R(w)|}{\|w\|} = \frac{|a(e, w)|}{\|w\|} = \frac{|a(e, \Pi w)|}{\|w\|} = \frac{|a(\Pi e, w)|}{\|w\|} \leq \|\Pi e\| \quad \forall w \in \mathcal{U}_0^h. \tag{21}$$

This proves that $\|\Pi e\|$ is an upper bound for the lower bound. The equality is achieved by setting $w = \Pi e$. Hence, the optimal lower bound takes the form $\|\Pi e\|$.

3.2.3 Influence of the surrogate conductivities on the error bounds

The homogenised conductivities $\bar{k}$ and $\hat{k}$ directly affect the sharpness of the error estimates in energy norm. The framework that we have developed so far allows us to characterise this sharpness, which provides insights that will prove useful when deriving bounds in QoIs. In particular, we show below that we can optimise analytically the upper bound by choosing particular surrogate conductivities. These optima turn out to coincide with variational bounds traditionally used in micromechanics to approximate the effective properties of composites.

Optimum result for the upper bound.   We show below how to choose $\hat{k}$ in order to maximise the effectivity of the upper bound, and how to choose $\bar{k}$ in order to minimise the error itself. These two optimisation processes are analytical and independent.

We start by noting that if we set $\bar{k}$, the conductivity of the temperature problem to $E[k]$ (rule of mixture), then the error in energy norm, $\|e\|$, is minimised. This is a direct outcome of the minimisation of $\|e\| = \|u - \bar{u}^h\|$ in the space of deterministic, kinematically admissible fields $\bar{u}^h$. This is shown by taking the first variation of $\|u - \bar{u}^h\|$ to obtain that in the stationary point,

$$a(\bar{u}^h, v) = a(u, v) = l(v) \quad \forall v \in \mathcal{U}_0. \tag{22}$$

Expanding $a(\bar{u}^h, v)$, and using the fact that both $\bar{u}^h$ and v are deterministic, we obtain

$$E\left[\int_\Omega k(\boldsymbol{x}, \theta) \, \nabla \bar{u}^h(\boldsymbol{x}) \cdot \nabla v(\boldsymbol{x}) \, d\Omega\right] = \int_\Omega E[k](\boldsymbol{x}) \, \nabla \bar{u}^h(\boldsymbol{x}) \cdot \nabla v(\boldsymbol{x}) \, d\Omega \tag{23}$$

Therefore, if $\bar{k} = E[k]$, it follows that $a(\cdot, \cdot) = \bar{a}(\cdot, \cdot)$ and that $\|e\|$ will be minimised.

This result can be seen as an extension of the Voigt assumption [40]. Indeed, in order to obtain analytical homogenised properties, Voigt constrains the strain field in an heterogeneous material to be constant. The resulting homogenised tensor is obtained by applying the rule of mixture. In our context, under the assumption that the temperature field is constant in the stochastic domain (deterministic), the reference temperature field u is best approached in norm $\|\cdot\|$ when using the rule of mixture.

A similar argument can be used to show that setting $\hat{k} = 1/E[k^{-1}]$ (inverse rule of mixture), will optimise the effectivity of the upper bound. This is an extension of Reuss' theory. In [31] it is shown that when assuming that the stress field is constant in an heterogeneous material, the resulting approximate effective tensor is the inverse rule of mixture (see also [43]). In our case, under the assumption that the flux field is deterministic, the solution of eq. (9) is best approximated using the inverse rule of mixture as the effective conductivity. Therefore, throughout the remainder of the paper, we set $\hat{k} = 1/E[k^{-1}]$.

Remark concerning the lower bound.   Choosing the rule of mixture as our surrogate conductivity, which minimises the error in energy norm, leads to a trivial lower bound. This can be shown by noting that,in this case,

$$\bar{a}(v, w) = a(v, w) \tag{24}$$

for any deterministic fields v and w. Hence, $R(v) = 0$ for any deterministic v, which leads to the lower bound $\|\Pi e\| = 0$. This can be seen as a result of Galerkin orthogonality. This is not directly useful, but the lower bound will prove essential to optimise the efficiency of error bounds in adaptive modelling.

Remark concerning the distance between upper and lower bound. We conclude this section with a result that will prove especially useful when dealing with error bounds for QoIs. We prove that the distance between the square of upper bond and the square of the lower bound,

$$\eta^2 - \|\Pi e\|^2 \tag{25}$$

does not depend on the conductivity field $\bar{k}$. Note that the previous expression is the uncertainty interval length for $\|e\|^2$, *i.e.*

$$\|\Pi e\|^2 \leq \|e\|^2 \leq \eta^2. \tag{26}$$

In order to show this, we observe that

$$\|e\|^2 = \|e - \Pi e\|^2 + \|\Pi e\|^2 \tag{27}$$

due to the orthogonality of $e - \Pi e$ and Πe, $a(e - \Pi e, \Pi e) = 0$. Hence, by expanding eq. (25)

$$\|\mathbf{e}^q\|^2_{k^{-1},\theta} + \|e\|^2 - \|\Pi e\|^2 = \|\mathbf{e}^q\|^2_{k^{-1},\theta} + \|e - \Pi e\|^2. \tag{28}$$

The proof is concluded by noting that in $e - \Pi e = u - \bar{u}^h + \Pi(u - \bar{u}^h) = u - \Pi u$, neither u, nor Πu depend on the field $\bar{k}$ [3].

3.3 Error bounds for quantities of interest

3.3.1 Error bounds for the expectation

In this section, we extend the bounds presented section 3.2 to quantities of interest. The techniques presented here are standard in the literature (see [5, 28] for discretisation error and for model error [20, 23–26, 32, 33, 39, 42]).

We start by introducing the following problems,

> For each $\theta \in \Theta$ and for all $v(\boldsymbol{x}) \in \mathcal{U}_0$, find $\phi(\boldsymbol{x}, \theta) \in \mathcal{U}_0$ such that,
>
> $$a_\theta(\phi, v) = q_\theta(v). \tag{29}$$

and its homogenised counterpart

> For all $v \in \mathcal{U}_0$, find $\bar{\phi} \in \mathcal{U}_0$
> $$\bar{a}(\bar{\phi}, v) = q(v) \tag{30}$$

where $q(v) = E[q_\theta(v)]$ is the QoI and $\bar{a}$ is the bilinear form defined eq. (3) with possibly a different homogenisation scheme. These problems are called dual problems, in contrast to eqs. (1) and (2) that are also called primal problems. A deterministic KA

---

[3]It is easy to see that $\bar{u}^h = \Pi u$ for $\bar{k} = E[k]$

approximation of $\bar{\phi}$ will be denoted by $\bar{\phi}^h$, while the SA approximation of its flux will be denoted by $\hat{\boldsymbol{q}}_\phi^h$. Using a standard procedure, we can show that,

$$q(u) - q(\bar{u}^h) = R(\bar{\phi}^h) + a(e, e_\phi) \tag{31}$$

where $e_\phi = \phi - \bar{\phi}^h$. Bounds for eq. (31) can be derived in at least two different ways. We review them both. Firstly, by applying Cauchy-Schwarz to the product of the errors, we obtain

$$R(\bar{\phi}^h) - \|e\|\|e_\phi\| \leq q(u) - q(\bar{u}^h) \leq R(\bar{\phi}^h) + \|e\|\|e_\phi\| \tag{32}$$

and using the bounds in energy-norm developed in section 3.2,

$$R(\bar{\phi}^h) - \eta\eta_\phi \leq q(u) - q(\bar{u}^h) \leq R(\bar{\phi}^h) + \eta\eta_\phi \quad \text{with } \|e_\phi\| \leq \eta_\phi. \tag{33}$$

Alternatively, bounds can be derived by noting that

$$a(e, e_\phi) = a(\alpha e, \, \alpha^{-1}e_\phi) \quad \forall \alpha \in \mathbb{R} \setminus \{0\} \tag{34}$$

and using the polarisation identity (as in [29]) to conclude that

$$q(u) - q(\bar{u}^h) = R(\phi^h) + \frac{\|\alpha e + \alpha^{-1}e_\phi\|^2 - \|\alpha e - \alpha^{-1}e_\phi\|^2}{4}. \tag{35}$$

Each of the terms $\|\alpha e \pm \alpha^{-1}e_\phi\|$ can be upper and lower bounded. Due to the bilinearity of $a(\cdot, \cdot)$, the bounds from section 3.2 can be applied to obtain,

$$(\eta_L^\pm)^2 \leq \|\alpha e \pm \alpha^{-1}e_\phi\|^2 \leq (\eta_U^\pm)^2 \tag{36}$$

where the following notation was used for compactness,

$$\eta_L^\pm := \|\alpha \Pi e \pm \alpha^{-1}\Pi e_\phi\|$$
$$\eta_U^\pm := \sqrt{E[\|\hat{\boldsymbol{q}}_{\alpha\pm}^h + k\nabla\bar{u}_{\alpha\pm}^h\|_{k^{-1},\theta}^2]}$$
$$\bar{u}_{\alpha\pm}^h := \alpha\bar{u}^h \pm \alpha^{-1}\bar{\phi}^h$$
$$\hat{\boldsymbol{q}}_{\alpha\pm}^h := \alpha\hat{\boldsymbol{q}}^h \pm \alpha^{-1}\hat{\boldsymbol{q}}_\phi^h$$

The results can be summarised in the following equation,

$$\underbrace{R(\bar{\phi}^h) - \frac{1}{4}(\eta_U^-)^2 + \frac{1}{4}(\eta_L^+)^2}_{=:\eta_{\text{Low}}^{\text{QoI}}} \leq q(u) - q(\bar{u}^h) \leq \underbrace{R(\bar{\phi}^h) + \frac{1}{4}(\eta_U^+)^2 - \frac{1}{4}(\eta_L^-)^2}_{=:\eta_{\text{Upp}}^{\text{QoI}}} \tag{37}$$

We set

$$\alpha = \sqrt[4]{\frac{\eta_\phi^2 - \|\Pi e_\phi\|^2}{\eta^2 - \|\Pi e\|^2}} \tag{38}$$

With this choice, the length of the interval is minimised. It is at most half of the interval length given by eq. (33). This is shown in detail in appendix A.1.

Remark 2. *We note that the bound in eq. (33) could be made sharper by considering it for a single realisation and then taking expectations. Indeed,*

$$q_\theta(u) - q_\theta(\bar{u}^h) \leq R_\theta(\bar{\phi}^h) + \|e\|_\theta\|e_\phi\|_\theta \leq \|\hat{\boldsymbol{q}}^h + k\bar{u}^h\|_{k^{-1},\theta}\|\hat{\boldsymbol{q}}_\phi^h + k\bar{\phi}^h\|_{k^{-1},\theta} \tag{39}$$

$$q(u) - q(\bar{u}^h) \leq R(\bar{\phi}^h) + E\left[\|\hat{\boldsymbol{q}}^h + k\bar{u}^h\|_{k^{-1},\theta}\|\hat{\boldsymbol{q}}_\phi^h + k\bar{\phi}^h\|_{k^{-1},\theta}\right] \tag{40}$$

It follows from the application of the Cauchy-Schwarz inequality to $E[\cdot]$ that,

$$E\left[\|\hat{\boldsymbol{q}}^h + k\bar{u}^h\|_{k^{-1},\theta}\|\hat{\boldsymbol{q}}_\phi^h + k\bar{\phi}^h\|_{k^{-1},\theta}\right] \leq \eta\eta_\phi. \tag{41}$$

However, this discussion does not extend to eq. (37). This follows from the fact that $(\eta_L^\pm)^2$ $(\eta_U^\pm)^2$ are left unchanged if independently computed for each realisation, followed by the computation of the expectation.

3.3.2 Choice of the homogenised conductivity

We readily observe that the uncertainty length for $q(e)$ in eq. (37),

$$\eta_{\text{Upp}}^{\text{QoI}} - \eta_{\text{Low}}^{\text{QoI}} = \frac{1}{4} \left[(\eta_U^+)^2 - (\eta_L^+)^2 + (\eta_U^-)^2 - (\eta_L^-)^2 \right] \tag{42}$$

is independent of the field $\bar{k}$. This is a consequence of the consideration in section 3.2.3 which shows that $\eta^2 - \|\Pi e\|^2$ is also a constant. In fact, the lower and upper bounds for $q(u)$,

$$q(\bar{u}^h) + \eta_{\text{Low}}^{\text{QoI}} \leq q(u) \leq q(\bar{u}^h) + \eta_{\text{Upp}}^{\text{QoI}} \tag{43}$$

are also independent of the field $\bar{k}$ (see appendix A.2 for the details). In conclusion, the choice of the $\bar{k}$ has no influence in the estimation of error in QoIs.

Regarding $\hat{k}$, the same consideration presented in section 3.2.3 applies and hence we set $\hat{k} = 1/E[k^{-1}]$.

Remark 3. *If $\bar{k} = E[k]$ in the primal problem and the same discretisation is used to solve eq. (30) (though not necessarily the same homogenisation scheme), then*

$$R(\bar{\phi}^h) = l(\bar{\phi}^h) - a(\bar{u}^h, \bar{\phi}^h) = l(\bar{\phi}^h) - \bar{a}(\bar{u}^h, \bar{\phi}^h) = 0 \tag{44}$$

since $\bar{\phi}^h \in \mathcal{U}_0^h$.

3.3.3 Error bound for the second moment

Following a similar methodology to the one presented in section 3.3.1, it can be shown that the second moment of the quantity of interest,

$$m_2 = E[q_\theta(u)^2], \tag{45}$$

is bounded by

$$m_2 - q(\bar{u}^h)^2 \leq (\gamma + \beta)^2 + 2\Delta[l(\bar{\phi}^h) + q(\bar{u}^h)] + l(\bar{\phi}^h)[R(\bar{\phi}^h) - a(\bar{u}^h, \bar{\phi}^h)] \tag{46}$$

under the non-restrictive assumption that $q(\bar{u}^h) > 0$ and $l(\bar{\phi}^h) > 0$ and where

$$\gamma = \sqrt{E\left[\int_\Omega k^{-1}(\hat{\boldsymbol{q}}^h + k\nabla\bar{u}^h)\,d\Omega \int_\Omega k^{-1}(\hat{\boldsymbol{q}}_\phi^h + k\nabla\bar{\phi}^h)\,d\Omega \right]} \tag{47}$$

$$\beta = \sqrt{E\left[\int_\Omega k\nabla\bar{u}^h \cdot \nabla\bar{\phi}^h \right]^2} \tag{48}$$

and Δ is an upper estimate for $q(e)$ from section 3.3.1. The complete result and a proof are given in appendix A.5.

The quantities β and γ are also deterministic. In other words, their computation does not involve the generation of realisations of the domain. This is shown by transforming the product of domain integrals into a double domain integral (see appendix A.5) by grouping together the stochastic terms (the conductivity and its reciprocal). The expectation of this term is related to the covariance function $\text{Cov}(k(x), k(x')) = E[k(x)k(x')] - E[k]^2$.

3.4 Adaptive modelling

Tighter error estimates can be obtained by solving the true model only in a subset of the domain. The resulting surrogate model is called adaptive model. In this section, we describe the obtention of the adaptive model and we introduce error indicators. Error indicators guide the construction of the adaptive model by signalling where the true model should be solved. The adaptive methodology followed here is similar to [32], though the proposed error estimates and error indicators differ.

We start by dividing the domain in N disjoint subdomains Ω_i, *i.e.*

$$\cup_{i=1}^{N} \Omega_i = \Omega \qquad \Omega_i \cap \Omega_j = \emptyset \quad (i \neq j). \tag{49}$$

This is followed by the computation of the error indicators for each of the subdomains. For the error in energy norm,

$$\eta_{\Omega_i}^2 = E\left[\int_{\Omega_i} k^{-1}(\hat{\boldsymbol{q}}^h + k\nabla\bar{u}^h)^2 \, d\Omega\right]. \tag{50}$$

Notice that the sum of the error indicators is equal to the upper bound,

$$\eta^2 = \sum_{i=1}^{N} \eta_{\Omega_i}^2 \tag{51}$$

The error indicator for the quantity of interest is given by

$$\beta_{\Omega_i}^2 = \frac{\alpha^2}{2} E\left[\int_{\Omega_i} k^{-1}(\hat{\boldsymbol{q}}^h + k\nabla\bar{u}^h)^2 \, d\Omega - \int_{\Omega_i} (\Pi e)^2 \, d\Omega\right] +$$
$$\frac{\alpha^{-2}}{2} E\left[\int_{\Omega_i} k^{-1}(\hat{\boldsymbol{q}}_\phi^h + k\nabla\bar{\phi}^h)^2 \, d\Omega - \int_{\Omega_i} (\Pi e_\phi)^2 \, d\Omega\right]. \tag{52}$$

In this case, their sum,

$$\eta_{\text{Upp}}^{\text{QoI}} - \eta_{\text{Low}}^{\text{QoI}} = \sum_{i=1}^{N} \beta_{\Omega_i}^2, \tag{53}$$

is equal to the interval length of eq. (37).

The subdomains Ω_i whose error indicators are above a certain user predefined tolerance are selected to be part of the adaptive model. Both error indicators, η_{Ω_i} and β_{Ω_i}, depend on the choice of the conductivity field. Nevertheless, in our numerical experiments the dependence was small enough to not change the domains selected for refinement.

Let W be the set of indexes of subdomains that are selected for refinement. We define the following pair of problems for each $w \in W$:

For each $\theta \in \Theta$ and for all $v \in \mathcal{U}_0(\Omega_w)$, find $\tilde{u}_{\Omega_w}(\boldsymbol{x}, \theta) \in \mathcal{U}(\Omega_w)$ such that

$$\int_{\Omega_w} k(\boldsymbol{x}, \theta)\, \nabla \tilde{u}_{\Omega_w}(\boldsymbol{x}, \theta) \cdot \nabla v(\boldsymbol{x}, \theta) = \int_{\Omega_w} f(\boldsymbol{x}) v(\boldsymbol{x}) \, d\Omega - \int_{\partial\Omega_w \cap \Gamma_N} g(\boldsymbol{x}) v(\boldsymbol{x}) \, d\Gamma. \tag{54}$$

---

where

$$\mathcal{U}(\Omega_w) = \{v \in H^1(\Omega_w) : v(\boldsymbol{x}) = \bar{u}^h(\boldsymbol{x}) \qquad \forall \boldsymbol{x} \in \partial\Omega_w \backslash \Gamma_N\}$$
$$\mathcal{U}_0(\Omega_w) = \{v \in H^1(\Omega_w) : v(\boldsymbol{x}) = 0 \qquad \forall \boldsymbol{x} \in \partial\Omega_w \backslash \Gamma_N\}.$$

For each $\theta \in \Theta$ and for all $p \in \mathcal{S}_0(\Omega_w)$, find $\tilde{\boldsymbol{q}}_{\Omega_w} \in \mathcal{S}(\Omega_w)$

$$\int_{\Omega_w} k^{-1}(\boldsymbol{x},\theta)\tilde{\boldsymbol{q}}_{\Omega_w}(\boldsymbol{x},\theta) \cdot \boldsymbol{p}(\boldsymbol{x})d\Omega = \int_{\partial\Omega_w \cap \Gamma_D} \boldsymbol{p}(\boldsymbol{x}) \cdot \boldsymbol{n}(\boldsymbol{x})\, h(\boldsymbol{x})d\Gamma \qquad (55)$$

where

$$
\begin{aligned}
\mathcal{S}(\Omega_w) = \{\boldsymbol{q} \in H^{\mathrm{div}}(\Omega_w) &: \boldsymbol{q}(\boldsymbol{x}) \cdot n(\boldsymbol{x}) = \hat{\boldsymbol{q}}^h(\boldsymbol{x}) && \forall \boldsymbol{x} \in \partial\Omega_w - \Gamma_D \\
&\text{and} \quad \nabla \cdot \boldsymbol{q}(\boldsymbol{x}) = f(\boldsymbol{x}) && \forall \boldsymbol{x} \in \Omega_w\}, \\
\mathcal{S}_0(\Omega_w) = \{\boldsymbol{q} \in H^{\mathrm{div}}(\Omega_w) &: \boldsymbol{q}(\boldsymbol{x}) \cdot n(\boldsymbol{x}) = 0 && \forall \boldsymbol{x} \in \partial\Omega_w - \Gamma_D \\
&\text{and} \quad \nabla \cdot \boldsymbol{q}(\boldsymbol{x}) = 0 && \forall \boldsymbol{x} \in \Omega_w\}.
\end{aligned}
$$

Since the field $\hat{\boldsymbol{q}}^h$ is SA, the problem in eq. (55) is well-posed.

Discrete KA and SA approximations $\tilde{u}_{\Omega_w}^h$ and $\tilde{\boldsymbol{q}}_{\Omega_w}^h$ are sought to the problems in combination with the Monte Carlo method. It is assumed that sufficient realisations are considered and for practical reasons, we have used a very fine KA approximation as $\tilde{\boldsymbol{q}}_{\Omega_w}^h$. As it will be seen in the examples, for fine meshes, the discretisation error is negligible when compared with the homogenisation error and consequently, the impact on the error bounds is negligible.

Using χ, the set indicator function, the approximations to the local problems can be combined to form the adaptive solution,

$$
\begin{aligned}
\tilde{u}^h &= \bar{u}^h + \sum_{w \in W} \chi_{\Omega_w}(\tilde{u}_{\Omega_w}^h - \bar{u}^h) \\
\tilde{\boldsymbol{q}}^h &= \hat{\boldsymbol{q}}^h + \sum_{w \in W} \chi_{\Omega_w}(\tilde{\boldsymbol{q}}_{\Omega_w}^h - \hat{\boldsymbol{q}}^h).
\end{aligned}
$$

Similarly, on the same subdomains, local approximations $\tilde{\phi}_{\Omega_w}^h$ and $\tilde{\boldsymbol{q}}_{\phi\Omega_w}^h$ of the dual true model are sought and used to build $\tilde{\phi}^h$ and $\tilde{\boldsymbol{q}}_\phi^h$. Note that $\tilde{u}^h$ and $\tilde{\phi}^h$ are kinematically admissible and $\tilde{\boldsymbol{q}}^h$ and $\tilde{\boldsymbol{q}}_\phi^h$ are statically admissible. Hence, the bounds presented in sections 3.2 and 3.3 can be immediately applied.

From an implementation point of view, we compute and store the restriction to the subdomains Ω_i of each of the terms that appear in the expression of the error bound, eq. (37). In other words, we calculate the quantities $R(\bar{\phi}^h)_{\Omega_i}$, $(\eta_L^\pm)^2_{\Omega_i}$ and $(\eta_U^\pm)^2_{\Omega_i}$ such that,

$$R(\bar{\phi}^h) = \sum_{i=1}^N R(\bar{\phi}^h)_{\Omega_i}, \quad (\eta_L^\pm)^2 = \sum_{i=1}^N (\eta_L^\pm)^2_{\Omega_i}, \quad (\eta_U^\pm)^2 = \sum_{i=1}^N (\eta_U^\pm)^2_{\Omega_i}. \qquad (56)$$

Those quantities can be combined to obtain the $\eta_{\mathrm{Low}}^{\mathrm{QoI}}$, $\eta_{\mathrm{Upp}}^{\mathrm{QoI}}$ and the error indicators. The refined error bounds can be obtained by recomputing $R(\bar{\phi}^h)_{\Omega_i}$, $(\eta_L^\pm)^2_{\Omega_i}$, and $(\eta_U^\pm)^2_{\Omega_i}$ only in the refined subdomains and using

$$
\begin{aligned}
R(\tilde{\phi}^h) &= R(\bar{\phi}^h) - \sum_{w \in W} \left(R(\bar{\phi}^h)_{\Omega_w} - R(\tilde{\phi}^h)_{\Omega_w}\right) \\
(\eta_L^\pm)^{2\prime} &= (\eta_L^\pm)^2 - \sum_{w \in W} \left((\eta_L^\pm)^2_{\Omega_w} - (\eta_L^\pm)^{2\prime}_{\Omega_w}\right) \\
(\eta_U^\pm)^{2\prime} &= (\eta_U^\pm)^2 - \sum_{w \in W} \left((\eta_U^\pm)^2_{\Omega_w} - (\eta_U^\pm)^{2\prime}_{\Omega_w}\right)
\end{aligned}
$$

where the prime indicates that quantity is related to the adaptive model.

14

Remark 4. *In [26], the authors prove the following alternative error bound (which is extended to QoIs in [33]),*

$$\|u - \tilde{u}\|^2 \leq 2[J(\tilde{u}) - J(\bar{u})] + \eta^2 \tag{57}$$

where

$$J(v) = \frac{1}{2}a(v, v) - l(v), \tag{58}$$

under the assumption that the discretisation errors are negligible. The drawback of this error bound is that it does not converge to 0 with model refinement. Indeed, by adding and subtracting $J(u)$ and using the identity, $\|u - v\|^2 = 2J(v) - 2J(u)$ (see [26]) for v KA,

$$\|u - \tilde{u}\|^2 \leq \|u - \tilde{u}\|^2 + E\left[\|\hat{\boldsymbol{q}} + k\nabla u\|^2_{k^{-1}}\right] \tag{59}$$

In other words, the effectivity of this bound is controlled by $\hat{\boldsymbol{q}}$, a field which is not affected by model refinement.

Remark 5. *An alternative error indicator for QoIs,*

$$\kappa_{\Omega_i} = \eta_{\Omega_i}\|\bar{\phi}^h\|_{\Omega_i} + \eta_{\Omega_i}\,\eta_{\phi\,\Omega_i} \tag{60}$$

where

$$\|\bar{\phi}^h\|_{\Omega_i} = E\left[\int_{\Omega_i} k\nabla\bar{\phi}^h \cdot \nabla\bar{\phi}^h\,d\Omega\right]$$

$$\eta_{\phi\,\Omega_i} = E\left[\int_{\Omega_i} k^{-1}(\hat{\boldsymbol{q}}^h_\phi + k\nabla\bar{\phi}^h)^2\,d\Omega\right].$$

was proposed in [25, 33]. Recalling eq. (33) and that $R(\bar{\phi}^h) = a(e, \bar{\phi}^h)$, it follows

$$q(u) - q(\bar{u}^h) \leq a(e, \bar{\phi}^h) + \eta\eta_\phi \leq \eta\|\bar{\phi}^h\| + \eta\eta_\phi. \tag{61}$$

The error bound follows from computing this upper bound for each subdomain.

However, we noticed that $R(\bar{\phi}^h)$ contributes to this indicator whilst this term does not affect the interval length as seen in eq. (33). As a consequence, the decrease of this term may not lead to a sharpening of the bound on the QoI (although the error itself would be decreased).

The error indicator presented in section 3.4 was built with the interval length in mind. It does not suffer from this conceptual problem. Another advantage of this error estimate is that its value is the maximum possible reduction of the error interval length when the respective subdomain is refined. This follows by considering that the all the subdomains not selected for refinement will contribute with the same quantity, while the subdomains refined will contribute with a non negative quantity.

Remark 6. *It is also interesting to remark that the introduction of the local approximations may increase the error bounds interval length. Notice that in these regions, the integrand of $\eta_L^\pm$ is 0. This reduction may not be compensated by the increase of sharpness of $\eta_U^\pm$.*

4　Numerical examples

In this section five numerical examples are presented. In the first example, the bounds are compared against a Monte Carlo reference solution of the heterogeneous problem. In the second example, we examine the effect of the contrast of the material properties and
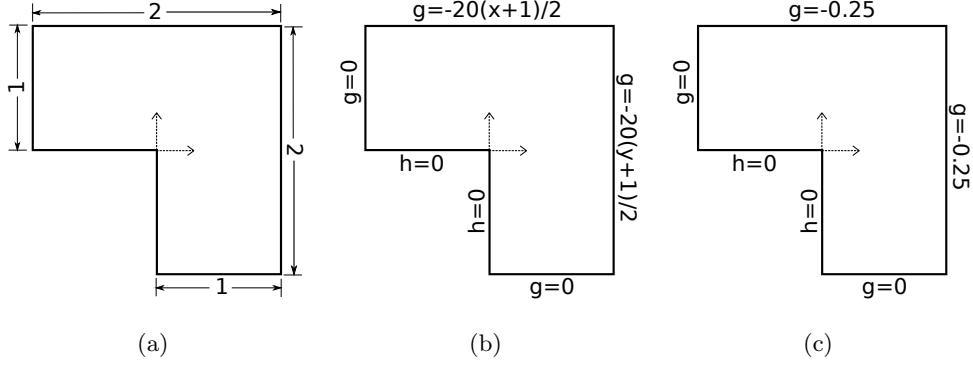
Figure 2: (a) Geometrical description of the domain, (b) boundary conditions for the primal and (c) dual problem in section 4.1.

the volume fraction in the bounds. The next example applies the bounds on a complex 3D geometry. This example is followed by a 1D numerical simulation where the bound for the second moment is applied. The section is concluded with an application of model adaptivity.

The meshes used were generated using Gmsh [9]. The code made extensive use of the library Eigen [11] and the post processing was done in ParaView [13].

4.1 Validation of the bounds

We compare the solution of a random heterogeneous problem with the bounds obtained from the homogenised problem. Since the random heterogeneous problem cannot be solved exactly, its solution is going to be approximated by an overkill Monte Carlo solution.

We consider the domain shown in figs. 2a and 2b. The source term, the prescribed fluxes and temperatures read

$$f(\boldsymbol{x}) = 0 \qquad \forall \boldsymbol{x} \in \Omega,$$

$$g(\boldsymbol{x}) = \begin{cases} -10(y+1) & \forall \boldsymbol{x} \in \{1\} \times [-1,1] \\ -10(x+1) & \forall \boldsymbol{x} \in [-1,1] \times \{1\} \\ 0 & \forall \boldsymbol{x} \in \{-1\} \times [0,1] \cup [0,1] \times \{-1\} \end{cases},$$

$$h(\boldsymbol{x}) = 0 \qquad \forall \boldsymbol{x} \in [-1,0] \times \{0\} \cup \{0\} \times [-1,0].$$

The quantity of interest is the average temperature on the external boundaries, $\omega = \{1\} \times [-1,1] \cup [-1,1] \times \{1\}$,

$$q(u) = \frac{1}{|\omega|} E\left[\int_\omega u d\Gamma\right].$$

In the domain, there are 75 circular particles of radius 0.05 and conductivity $k_p = 0.5$. The matrix has a conductivity of $k_m = 1$. Consequentially, the volume fraction is approximately $\nu = 0.196$. The centres of the particles are placed following a uniform distribution over the domain and not allowing them to intersect with other particles or the boundaries of the domain. An approximation to the solution of this problem is built by using the finite element method with 512 Monte Carlo realisations. The resulting histogram of the quantity of interest is shown in fig. 3.

16

To compute bounds, we approximate the probability of a point being inside a particle for any point of the domain by the volume fraction[4], hence $E[k] \approx k_p \nu + (1 - \nu) k_m$. Our approximations will be compared with the a posteriori bound from the section 3. The kinematically admissible approximations are obtained using $\bar{k} = E[k]$ as homogenised conductivity, while we use $\hat{k} = 1/E[k^{-1}]$ as the homogenised conductivity for the statically admissible solution schemes. The same mesh is used for all approximations and it is shown in fig. 4a.

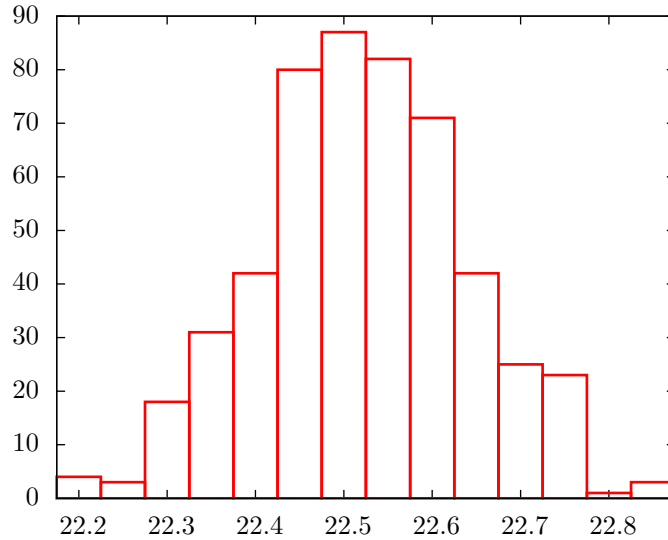We note that in this case, the adjoint problem has a physical interpretation which is shown in fig. 2c.

Figure 3: Histogram of the quantity of interest from section 4.1. Mean: 22.55 Std. deviation: 0.12.

The results are summarised in table 1 and figs. 4 and 5. We see that the bounds hold and that they are sharp. We see that the ratio between error interval length and exact QoI oscillates between 0.08 and 0.16. The alternative measure, the ratio between error interval and the error in the QoI is not a good choice to evaluate the sharpness of the bounds, since the interval length of *eq.* (37) is independent of $\bar{k}$ whilst $q(e)$ depends on it. We also mention that in this specific example, the effect of neglecting the discretisation errors and using a KA field as an SA field does not have an important influence on the bounds as we can see on the results. In fact, the discretisation error can be computed by considering eq. (2) as the true model. By applying the bound in eq. (33), we obtain,

$$|q(\bar{u}) - q(\bar{u}^h)| \leq 0.016. \tag{62}$$

which is negligible when compared to the total error.

4.2 Effects of the volume fraction and material contrast

The domain considered for this study is shown in fig. 6. The conductivity of the matrix is fixed to the value $k_m = 1$, while the conductivity of the inclusions, k_p will take the values 0.25, 0.5 and 0.75. These problems are solved for volume fractions ν equal to 0.1,

---

[4]As the domain increases and the no. of particles increase accordingly while their size remain constant, the error becomes negligible.
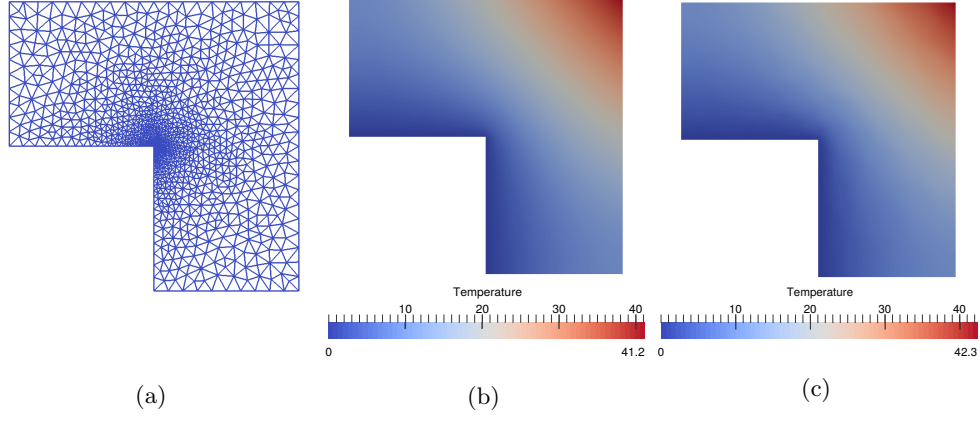
Figure 4: (a)Mesh used for the homogeneous problem. 2066 linear triangular elements (b) The temperature field of the compatible solution (c) The temperature field of one realisation (section 4.1).
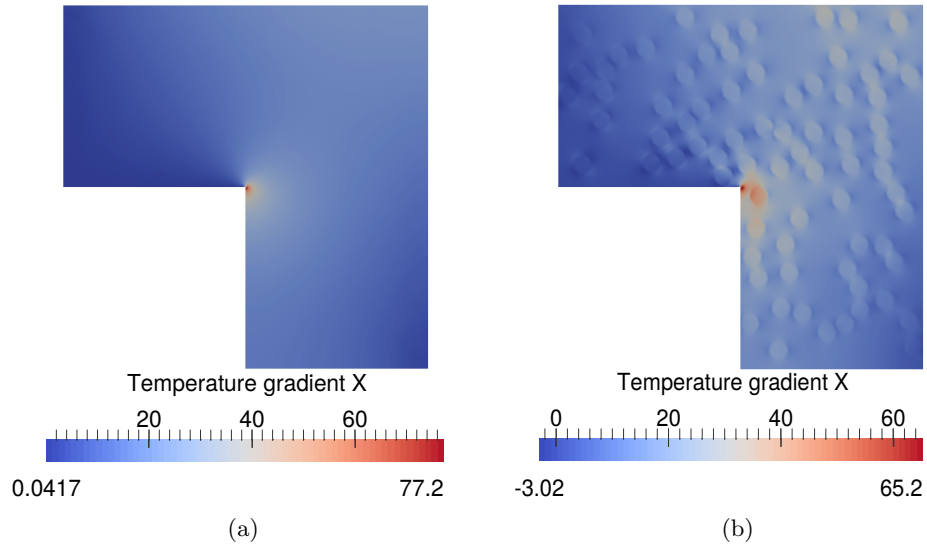

Figure 5: (a) The temperature gradient in X direction of the compatible solution (b) The temperature gradient in X direction of a realisation (section 4.1).

$q(\bar{u}^h)$	ζ_l	$q(u) - q(\bar{u}^h)$	ζ_u	$\zeta_l + q(\bar{u}^h)$	$q(u)$	$\zeta_u + q(\bar{u}^h)$
	-1.842		1.842	20.08		23.76
21.92	-0.0483	0.63	1.794	21.87	22.55	23.71
	-1.822		1.822	20.1		23.74

Table 1: Results from section 4.1. ζ_l and ζ_u represent both lower and upper bounds respectively. The first row shows the results for the error bound in eq. (33) and the second row for the error bound in eq. (37). In the third row, it was assumed that the discretisation error is negligible and a KA approximation was used as a SA field. The bound applied was the one in eq. (33).
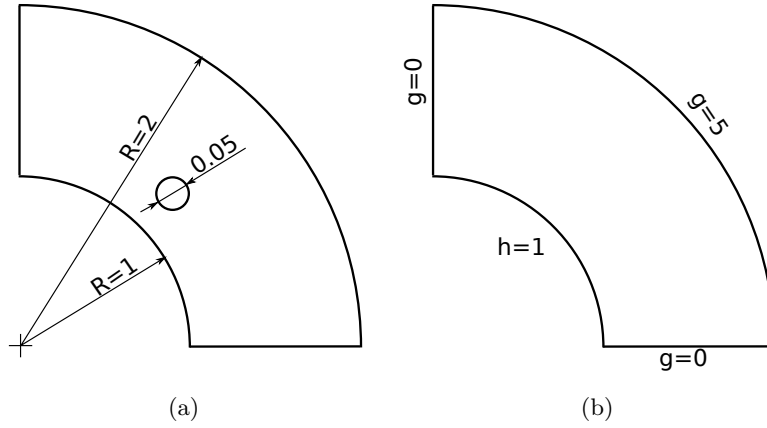

Figure 6: Description of the problem from section 4.2 (a) Geometry of the domain. The coordinates of the centre of the circle are $(\sqrt{0.75}, \sqrt{0.75})$. The quantity of interest is the average temperature in this circle. (b) Boundary conditions.

0.2 and 0.3. We assume that the probability of being inside a particle is a constant and coincides with the volume fraction. Under this assumption $E[k] = \nu k_p + (1 - \nu)k_m$ and $E[k^{-1}] = \nu/k_p + (1 - \nu)/k_m$. The results were restricted to the bounds in eq. (37). The KA approximations are obtained using rule of mixture $E[k]$, while the SA approximations are obtained using inverse rule of mixture $1/E[k^{-1}]$. In fig. 6, the mesh used in the analysis is shown together with the resulting primal and dual temperature field. The primal homogenised solution is radial in its nature while the dual homogenised solution peaks in the region of interest due to the induced source term. The bounds are plotted in fig. 8 and their numerical values are summarised in table 2.

The results show that as we increase the material contrast and/or the volume fraction, the interval defined by the error bounds grows in length. This example highlights one of the limitations of this work, high material contrasts can increase drastically the interval defined by the bounds. In the appendix A.3, we present a discussion regarding this behaviour.

4.3 Complex 3D example

We consider in this example a complex 3D domain. The methodology is applied to the cylinder head of an engine(fig. 9). At the bottom of the cylinder a temperature of $460K$ is prescribed. At the fins and the upper face it is assumed that a flux of $200W \cdot m^{-2}$ exits the body, while it is assumed that there is no heat exchange in the hole and lateral
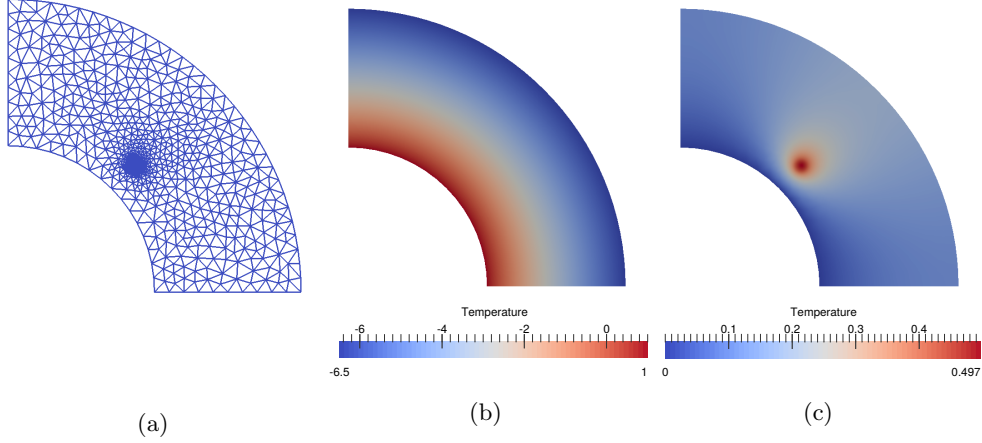
Figure 7: Results of the problem from section 4.2 (a) Linear triangular mesh composed of 1412 elements used for the simulation (b) Temperature field of the primal problem for a conductivity of 0.25 and a volume fraction of 0.1 (c) Temperature field of the dual problem for a conductivity of 0.25 and a volume fraction of 0.1

ν	k_i	$q(\bar{u}^h)$	$\zeta_l + q(\bar{u}^h)$	$\zeta_u + q(\bar{u}^h)$	$\zeta_u - \zeta_l$
0.1	0.25	-1.18672	-2.17531	-0.646484	1.52882
0.1	0.5	-1.12935	-1.36253	-0.997478	0.365049
0.1	0.75	-1.07491	-1.1297	-1.04107	0.0886278
0.2	0.25	-1.3791	-3.26921	-0.351572	2.91764
0.2	0.5	-1.24729	-1.66483	-1.01533	0.6495
0.2	0.75	-1.12935	-1.21403	-1.07858	0.135452
0.3	0.25	-1.60872	-4.3196	-0.137407	4.1822
0.3	0.5	-1.3791	-1.95062	-1.06355	0.887065
0.3	0.75	-1.18672	-1.29409	-1.12329	0.170796

Table 2: Results from the section 4.2. ζ_u and ζ_l are the lower and upper bounds in eq. (37). The last column presents the interval length.

surfaces. The body is made of matrix enriched with particles. The thermal conductivity of the matrix is $460W/(m \cdot K)$, while the conductivity of the inclusions is $230W/(m \cdot K)$. The inclusions add up to 20% of the volume of the domain. Again, we assume that $E[k] = \nu k_p + (1 - \nu)k_m$ and $E[k^{-1}] = \nu/k_p + (1 - \nu)/k_m$. The quantity of interest is the average temperature on the upper face. The domain was discretised with roughly 1.5 million linear tetrahedrons. The KA approximations were obtained using rule of mixture $E[k]$, while the SA approximations were obtained using inverse rule of mixture $1/E[k^{-1}]$. The resulting temperature field can be seen in fig. 10 while the bounds can be found in table 3. The bounds are sharp if compared to the temperatures present in the problem (≈ 450). The resulting interval length of the bound in eq. (37), 1.5, is half of the interval length resulting from eq. (33), 3. This relation between both bounds is explained in appendix A.1.
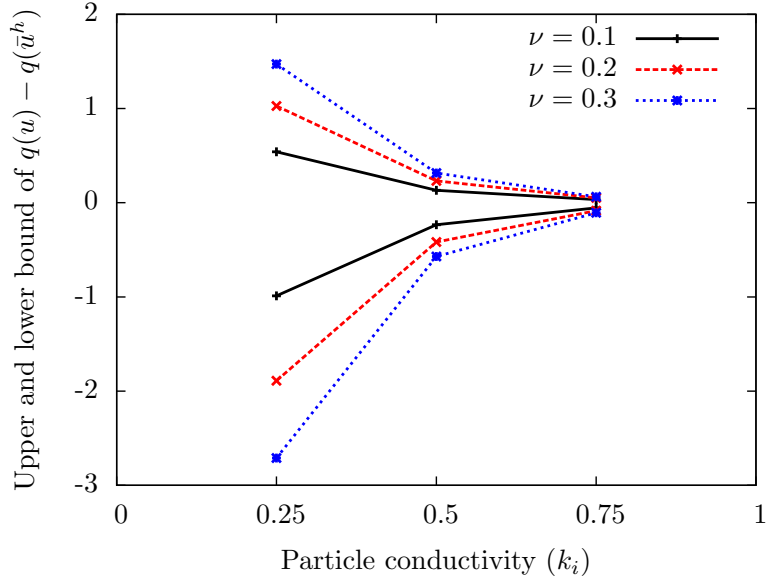
20

Figure 8: Effect of the contrast of conductivities in the lower and upper bound. From section 4.2.
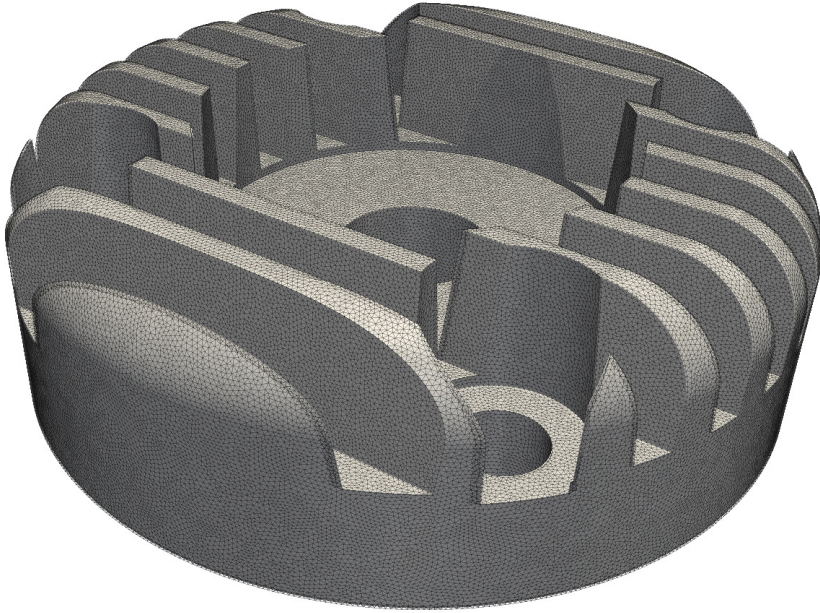

Figure 9: Cylinder head (section 4.3)

4.4 Validation of the bound for the second moment

The purpose of this numerical example is to validate the bound for the second moment presented in section 3.3.3. We consider an unidimensional domain defined on the interval $[0, 8]$. In the domain, there are 4 particles of length of 0.5 with unknown position. Their conductivity is 0.5 and the conductivity of the rest of the domain is 1. At both ends of
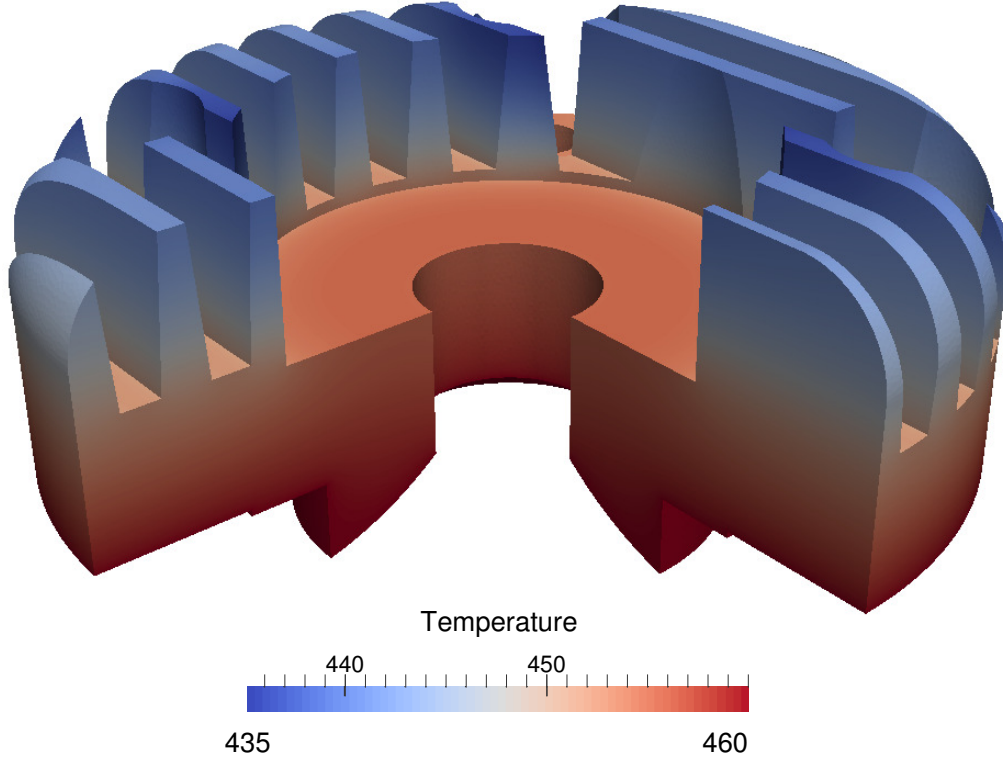
Figure 10: Temperature field of the cylinder head(section 4.3)

$q(\bar{u}^h)$	ζ_l	$q(u) - q(\bar{u}^h)$	ζ_u	$\zeta_l + q(\bar{u}^h)$	$q(u)$	$\zeta_u + q(\bar{u}^h)$
	-1.506		1.506	444.3		447.3
445.8	-1.503	?	0.002728	444.3	?	445.8
	-1.085		1.085	444.7		446.9

Table 3: Results from section 4.3. ζ_l and ζ_u represent both lower and upper bounds respectively. The first row corresponds to the error bound in eq. (33) and the second row corresponds to the error bound in eq. (37). In the third row, it was assumed that the discretisation error is negligible and a KA approximation was used as a SA field. The bound applied was the one in eq. (33).

the domain, the temperature is set to 0. The source term is $f(x) = -1$. The quantity of interest is the average temperature in the interval $[0.45, 0.5]$.

The centres of the particles are placed following an uniform distribution in the domain. The particles are not allowed to intersect with each other, however, when they intersect with the boundary, the exceeding part of the particle is placed on the other end of the domain. This results in a probability of being inside of a particle of 0.25 for all points of
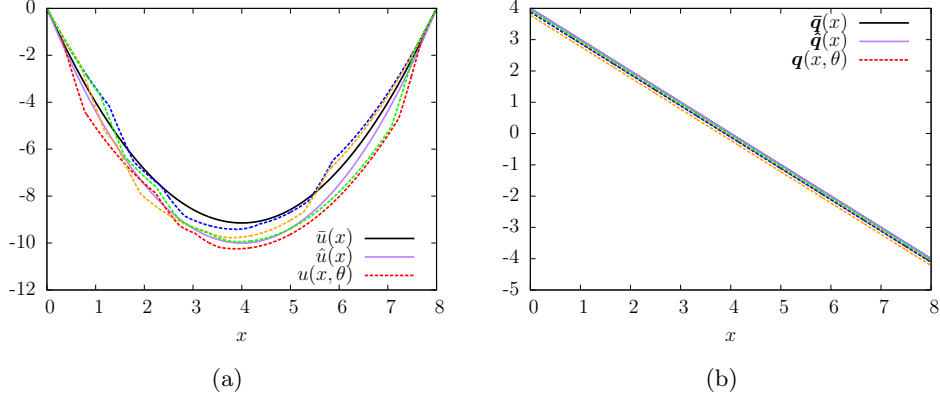
22

Figure 11: (a) The temperature field of the homogenised solution and four realisations. Notice its independence of the homogenisation scheme (b) The flux field of the homogenised solution and of the exact solution.

$q(u)$	-2.23	m_2	5.31
$q(\bar{u}^h)$	-2.04	$q(\bar{u}^h)^2$	4.16
ζ_l	-0.33	ζ_2	9.92
ζ_u	0.013		

Table 4: Summary of the results of section 4.4. The exact quantity of interest was approximated by the solution of 2096 realisations of the problem. ζ_l and ζ_u are lower and upper bounds for $q(e)$ respectively. ζ_2 is an upper bound for m_2 (see section 3.3.3) .

the domain and that coincides with the volume fraction.

The KA and SA surrogate models are built by setting $\bar{k} = E[k]$ and $\hat{k} = 1/E[k^{-1}]$. The surrogate models and several realisations are shown in fig. 11. Bounds for the expectation and the second moment of the quantity of interest are computed using eqs. (37) and (46).

To compute the bounds for the second moment, we need the fields $E[k(x)k(y)]$, $E[k^{-1}(x)k(y)]$ and $E[k^{-1}(x)k^{-1}(y)]$. Those functions are computed using the auxiliary probability functions $p_i(d)$, $p_o(d)$ and $p_d(d)$. Given two points separated by a distance d: $p_i(d)$ is the probability that both points are inside a particle, $p_o(d)$ is the probability of both points being in the matrix, and $p_d(d)$ is the probability of one point being inside a particle and the other being in the matrix. These functions were computed numerically by generating 50000 realisations of the domain. In fig. 12 their numerical approximation is shown. Once those functions are available, we can compute

$$E[k(x)k(y)] = k_i^2 p_i(|x - y|) + k_m^2 p_o(|x - y|) + k_i k_m p_d(|x - y|) \qquad (63)$$

and similarly for $E[k^{-1}(x)k^{-1}(y)]$ and $E[k(x)k^{-1}(y)]$.

All the results are summarised in table 4. The bounds for the expectation hold and they were computed using eq. (37). The ratio between the interval length and $q(u)$ is 0.15. The bound for the second moment also holds but it is not very sharp. In this case the ratio between the bound and the exact second moment m_2 is 1.87. This is expected due to the inequalities used in the derivation of the bound that rely on the effectivity of the bound for the expectation.
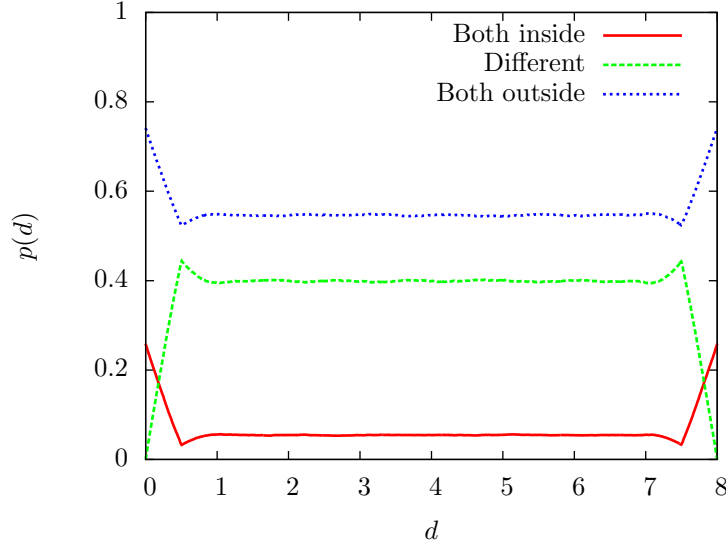
23

Figure 12: Probability of two points separated a distance x being both inside a particle (Both inside), both in the matrix (Both outside) and one being inside a particle and one inside the matrix (Different). Computed using 50000 realizations of the domain.

4.5 Adaptive modelling example

In this example, we apply the ideas presented in section 3.4. The domain is described in fig. 13. The domain is an aggregate of two constituents, round particles (radius 0.04, conductivity 5) surrounded by a matrix (conductivity 1). There are 740 particles and the centre of the particles behaves like a uniform random variable inside the domain. They are not allowed to intersect each other, but are allowed to intersect the boundaries. The average volume fraction is $\nu = 0.189$ and we assume that $E[k] = \nu k_p + (1 - \nu)k_m$ and $E[k^{-1}] = \nu/k_p + (1 - \nu)/k_m$. We set $\hat{k} = 1/E[k^{-1}]$, while we will set $\bar{k}$ to 11 equally spaced values in the interval $[1/E[k^{-1}], E[k]]$.

The domain is further subdivided in 8 squares which naturally align with the edges of the interior void. The corresponding error estimators are shown in table table 5. We note that the difference between the estimators for different $\bar{k}$ is small. Subdomain 2, the area below the void, is selected for refinement. The bounds are computed using the technique described in section 3.4. Figure 15 remarks the importance of the choice of the conductivity in order to optimise the uncertainty gap. Without model refinement, the uncertainty gap is

$$-7.60118 \le q(u) \le -4.25279 \tag{64}$$

This is independent of $\bar{k}$. With model refinement, the smallest uncertainty gap for $q(u)$,

$$-7.26408 \le q(u) \le -4.48026 \tag{65}$$

is attained when $\bar{k} = 1.47$. The homogenised temperature field and a realisation of the window are shown in fig. 14. In this case, the interval length reduction is equal 0.56, value close to the error indicator in the subdomain, 0.64. This means that, as mentioned in remark 5, we have reduced the uncertainty in the QoI by an amount close to what we consider to be a "theoretical maximum". We also note that for small $\bar{k}$, the lower bound for the adaptive model is worst than the original as explained in remark 6. Finally, the upper bound for error in energy norm η ($\bar{k} = 1.47$), takes the value 4.938 before model

24

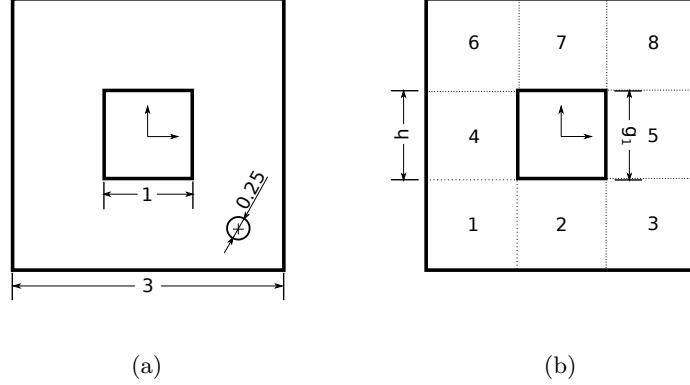(a)   (b)

Figure 13: Description of the problem from section 4.5 (a) Geometry of the domain. The coordinates of the centre of the circle are $(1, -1)$. The quantity of interest is the average temperature in this circle. (b) Boundary conditions and subdomain numbering. $h = 0$ and $g_1 = 40(0.5 + y)(0.5 - y)$ on the indicated regions. $g = 0$ in the rest of the boundary.

Ω_i	β_{Ω_i}	Ω_i	β_{Ω_i}
1	0.4405	5	0.4973
2	0.6359	6	0.2852
3	0.3646	7	0.3872
4	0.5809	8	0.1568

Table 5: Local error indicators for the QoI ($\bar{k} = 1.47$). Subdomain 2 contributes most to the error in the QoI and it is selected for model refinement.

refinement and 4.576 after model refinement. Using the bound mentioned in remark 4, the value is 4.669. The difference between both bounds is small, though, it could be magnified in other problems.

5   Conclusion

We have presented a new approach to guarantee the accuracy of homogenisation schemes for random heterogeneous media through error bounding. Our approach combines two novel points: (i) the description of the microscopic model as a stochastic problem where the position of the heterogeneities are described by random variables, and (ii) the development of an error bounding framework based on the Prager-Synge hypercircle theorem. The first of these points has allowed to to eliminate the need for microscopic operations when calculating error estimates, thereby extending the applicability of upscaling error bounding to the modelling of composites with arbitrary scale ratios: we have retrieved a "numerical scale separation".

The second point has allowed us to fully characterise the efficiency of the error estimators and to interpret them as an extension of Reuss-Voigt bounds to macroscale engineering quantities of interest. Compared to the state-of-the-art, this new framework has allowed us to obtain optimally sharp error bounds, meaning that the remaining uncertainty on the QoI is as small as possible when using deterministic primal/dual homogeneous surrogates as computable approximate solutions to intractable microscopic
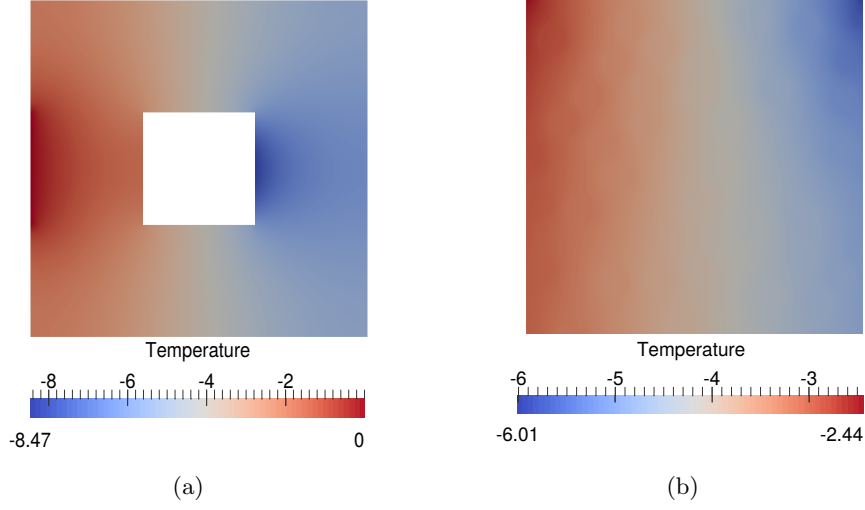
Figure 14: (a) Temperature field of the surrogate model for $\bar{k} = 1.47$. (b) A realisation of the local approximation.
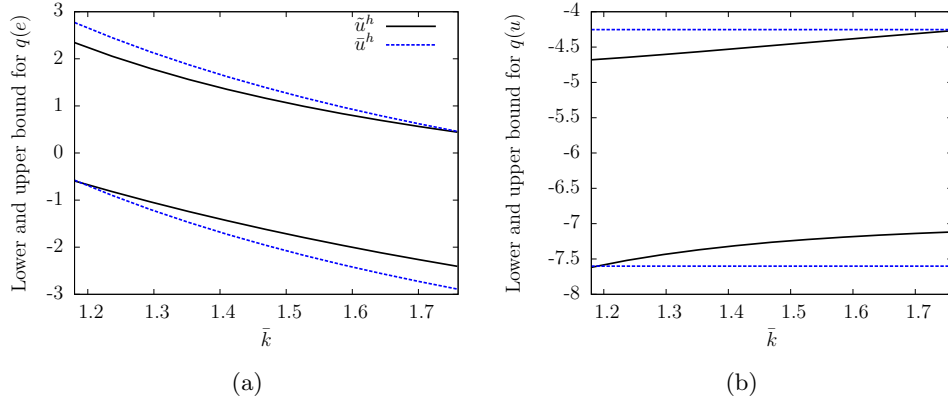

Figure 15: Lower and upper bounds for the solution $\bar{u}^h$ to the purely macroscopic problem and for the solution $\tilde{u}^h$ for the adaptive model as a function of the surrogate conductivity $\bar{k}$. The graph on the left-hand side presents the bounds for the error in QoI, while the graph on the right-hand side presents the bound for the QoI itself.

problem. In practical terms, the error bounds are trivial to implement, and require only a small overhead compared to the direct application of homogenisation schemes. However, obtaining strict guarantees has required us to implement a Stress Finite Element method, which is not a standard formulation in the computational mechanics community.

Our approach has been applied successfully to several numerical examples and a strategy was developed to adaptively control the sharpness of the bounds through local model adaptivity. The extension of the results to other linear elliptic problems such as linear elasticity should be straightforward.

The main limitation of our methodology is the fast increase in the uncertainty on QoIs as the contrast between the material properties increases. This property is intuitively related to the Reuss-Voigt character of the bounds that we have derived. We believe that a way (actually the only way) to circumvent this limitation is to allow our primal and dual surrogate solutions to globally fluctuate in the stochastic space, which would automatically result in the decrease of both the error in energy norm and of the effectivity of the associated error bound. However, it seems tremendously difficult to find a space of tractable finite dimension that would represent the microscopic fluctuation of the "true" solution with sufficient accuracy. We are currently working on this fundamental issue. We also acknowledge the fact that the method at the present state is only able to characterise the first two moments of the quantity of interest while in certain circumstances a full description of the probability density function might be required.

Acknowledgements

References

[1] A. Abdulle and A. Nonnenmacher. Adaptive finite element heterogeneous multiscale method for homogenization problems. *Computer Methods in Applied Mechanics and Engineering*, 200(37-40):2710–2726, 2011.

[2] Mark Ainsworth and J Tinsley Oden. *A posteriori error estimation in finite element analysis*, volume 37. John Wiley & Sons, 2011.

[3] Ahmad Akbari Rahimabadi, Pierre Kerfriden, and Stéphane Bordas. Scale selection in nonlinear fracture mechanics of heterogeneous materials. *Philosophical Magazine*, 95(28-30):3328–3347, oct 2015.

[4] Ivo Babuška, Raúl Tempone, and Georgios E. Zouraris. Solving elliptic boundary value problems with uncertain coefficients by the finite element method: the stochastic formulation. *Computer Methods in Applied Mechanics and Engineering*, 194(12-16):1251–1294, apr 2005.

[5] Roland Becker and Rolf Rannacher. *A feed-back approach to error control in finite element methods: Basic analysis and examples*. Citeseer, 1996.

[6] Ludovic Chamoin and Pedro Diez. *Verifying Calculations-Forty Years On: An Overview of Classical Verification Techniques for FEM Simulations*. Springer, 2015.

[7] J.P.Moitinho de Almeida and J.A.Teixeira de Freitas. Alternative approach to the formulation of hybrid equilibrium finite elements. *Computers & Structures*, 40(4):1043–1047, jan 1991.

[8] Pedro Díez, Núria Parés, and Antonio Huerta. Error Estimation and Quality Control. In *Encyclopedia of Aerospace Engineering*. John Wiley & Sons, Ltd, Chichester, UK, dec 2010.

[9] Christophe Geuzaine and Jean-François Remacle. Gmsh: A 3-d finite element mesh generator with built-in pre-and post-processing facilities. *International Journal for Numerical Methods in Engineering*, 79(11):1309–1331, 2009.

[10] Roger G Ghanem and Pol D Spanos. *Stochastic finite elements: a spectral approach*. Courier Corporation, 2003.

[11] Gaël Guennebaud, Benoît Jacob, et al. Eigen v3. http://eigen.tuxfamily.org, 2010.

[12] Z. Hashin and S. Shtrikman. A variational approach to the theory of the elastic behaviour of multiphase materials. *Journal of the Mechanics and Physics of Solids*, 11(2):127–140, mar 1963.

[13] Amy Henderson, Jim Ahrens, Charles Law, et al. *The ParaView Guide*. Kitware Clifton Park, NY, 2004.

[14] Pierre Ladevèze and Eric Florentin. Verification of stochastic models in uncertain environments using the constitutive relation error method. *Computer methods in applied mechanics and engineering*, 196(1):225–234, 2006.

[15] Pierre Ladevèze and Dominique Leguillon. Error estimate procedure in the finite element method and applications. *SIAM Journal on Numerical Analysis*, 20(3):485–509, 1983.

[16] Pierre Ladevèze, Jean-Pierre Pelle, Frederick F Ling, Ernest F Gloyna, and William Howard Hart. *Mastering calculations in linear and nonlinear mechanics*. Springer, 2005.

[17] Fredrik Larsson and Kenneth Runesson. On two-scale adaptive FE analysis of micro-heterogeneous media with seamless scale-bridging. *Computer Methods in Applied Mechanics and Engineering*, 200(37-40):2662–2674, 2011.

[18] S. Loehnert, C. Prange, and P. Wriggers. Error controlled adaptive multiscale XFEM simulation of cracks. *International Journal of Fracture*, 178(1-2):147–156, 2012.

[19] H.G. Matthies. Stochastic finite elements: Computational approaches to stochastic partial differential equations. *ZAMM*, 88(11):849–873, nov 2008.

[20] Nicolas Moës, J.Tinsley Oden, and Tarek I. Zohdi. Investigation of the interactions between the numerical and the modeling errors in the Homogenized Dirichlet Projection Method. *Computer Methods in Applied Mechanics and Engineering*, 159(1-2):79–101, jul 1998.

[21] T Mori and K Tanaka. Average stress in matrix and average elastic energy of materials with misfitting inclusions. *Acta metallurgica*, 21(5):571–574, 1973.

[22] Sia Nemat-Nasser and Muneo Hori. *Micromechanics: overall properties of heterogeneous materials*. Elsevier, 2013.

[23] J. Tinsley Oden, Kumar Vemaganti, and Nicolas Moës. Hierarchical modeling of heterogeneous solids. *Computer Methods in Applied Mechanics and Engineering*, 172(98):3–25, 1999.

[24] J.Tinsley Oden and Serge Prudhomme. Estimation of Modeling Error in Computational Mechanics. *Journal of Computational Physics*, 182(2):496–515, nov 2002.

[25] J.Tinsley Oden and Kumar S. Vemaganti. Estimation of Local Modeling Error and Goal-Oriented Adaptive Modeling of Heterogeneous Materials. *Journal of Computational Physics*, 164(1):22–47, oct 2000.

[26] J.Tinsley Oden and Tarek I. Zohdi. Analysis and adaptive modeling of highly heterogeneous elastic structures. *Computer Methods in Applied Mechanics and Engineering*, 148(3-4):367–391, sep 1997.

[27] William Prager and John L Synge. Approximations in elasticity based on the concept of function space. *Quart. Appl. Math*, 5(3):241–269, 1947.

[28] S. Prudhomme and J.T. Oden. On goal-oriented error estimation for elliptic problems: application to the control of pointwise errors. *Computer Methods in Applied Mechanics and Engineering*, 176(1-4):313–331, jul 1999.

[29] Serge Prudhomme and J Tinsley Oden. On goal-oriented error estimation for elliptic problems: application to the control of pointwise errors. *Computer Methods in Applied Mechanics and Engineering*, 176(1):313–331, 1999.

[30] P. Raghavan and S. Ghosh. *Concurrent multi-scale analysis of elastic composites by a multi-level computational model*, volume 193. 2004.

[31] A Reuss. Berechnung der fließgrenze von mischkristallen auf grund der plastizitätsbedingung für einkristalle. *ZAMM-Journal of Applied Mathematics and Mechanics/Zeitschrift für Angewandte Mathematik und Mechanik*, 9(1):49–58, 1929.

[32] Albert Romkes, J. Tinsley Oden, and Kumar Vemaganti. Multi-scale goal-oriented adaptive modeling of random heterogeneous materials. *Mechanics of Materials*, 38(8-10):859–872, aug 2006.

[33] Albert Romkes, Kumar Vemaganti, and JT Oden. The extension of the GOALS algorithm to the analysis of elastostatics problems of random heterogeneous materials. *ICES Report*, (September), 2004.

[34] Enrique Sanchez-Palencia and André Zaoui. Homogenization techniques for composite media. In *Homogenization Techniques for Composite Media*, volume 272, 1987.

[35] Erwin Stein and Marcus Rüter. Finite Element Methods for Elasticity with Error-controlled Discretization and Model Adaptivity. In *Encyclopedia of Computational Mechanics*. John Wiley & Sons, Ltd, Chichester, UK, oct 2007.

[36] M. Steven Greene, Yu Liu, Wei Chen, and Wing Kam Liu. Computational uncertainty analysis in multiresolution materials via stochastic constitutive theory. *Computer Methods in Applied Mechanics and Engineering*, 200(1-4):309–325, jan 2011.

[37] İ. Temizer, T. Wu, and P. Wriggers. On the optimality of the window method in computational homogenization. *International Journal of Engineering Science*, 64:66–73, mar 2013.

[38] Salvatore Torquato. *Random heterogeneous materials: microstructure and macroscopic properties*, volume 16. Springer Science & Business Media, 2013.

[39] Kumar S. Vemaganti and J.Tinsley Oden. Estimation of local modeling error and goal-oriented adaptive modeling of heterogeneous materials. *Computer Methods in Applied Mechanics and Engineering*, 190(46-47):6089–6124, sep 2001.

[40] Woldemar Voigt. Ueber die beziehung zwischen den beiden elasticitätsconstanten isotroper körper. *Annalen der Physik*, 274(12):573–587, 1889.

[41] O. C. Zienkiewicz. Displacement and equilibrium models in the finite element method by B. Fraeijs de Veubeke, Chapter 9, Pages 145–197 of Stress Analysis, Edited by O. C. Zienkiewicz and G. S. Holister, Published by John Wiley & Sons, 1965. *International Journal for Numerical Methods in Engineering*, 52(3):287–342, sep 2001.

[42] Tarek I. Zohdi, J.Tinsley Oden, and Gregory J. Rodin. Hierarchical modeling of heterogeneous bodies. *Computer Methods in Applied Mechanics and Engineering*, 138(1-4):273–298, dec 1996.

[43] Tarek I Zohdi and Peter Wriggers. *An introduction to computational micromechanics.* Springer Science & Business Media, 2008.

A   Appendices

A.1   Optimal value of α

The optimal value of α minimises $f(\alpha) := \eta_{\mathrm{Upp}}^{\mathrm{QoI}} - \eta_{\mathrm{Low}}^{\mathrm{QoI}}$, the uncertainty interval length. Through algebraic manipulations, we obtain

$$f(\alpha) = \frac{1}{4} \left[(\eta_U^+)^2 - (\eta_L^+)^2 + (\eta_U^-)^2 - (\eta_L^-)^2 \right]$$

$$(\eta_U^\pm)^2 = \|\hat{\boldsymbol{q}} + k\nabla\bar{u}^h\|_{k^{-1}}^2 \alpha^2 + \|\hat{\boldsymbol{q}}_\phi + k\nabla\bar{\phi}^h\|_{k^{-1}}^2 \alpha^{-2}$$
$$\pm 2E\left[\int_\Omega k^{-1}(\hat{\boldsymbol{q}} + k\nabla\bar{u}^h)(\hat{\boldsymbol{q}}_\phi + k\nabla\bar{\phi}^h) \, d\Omega \right]$$

$$(\eta_L^\pm)^2 = \alpha^2 \|\Pi e\| + \alpha^{-2} \|\Pi e_\phi\| \pm 2a(\Pi e, \Pi e_\phi).$$

Hence,

$$f(\alpha) = \frac{1}{4}[2\alpha^2(\eta^2 - \|\Pi e\|^2) + 2\alpha^{-2}(\eta_\phi^2 - \|\Pi e_\phi\|^2)]. \tag{66}$$

Since f is even, we can assume $\alpha > 0$. Then, the minimum is attained when the first derivative is cancelled

$$f'(\alpha_{\mathrm{opt}}) = 0 \Leftrightarrow \alpha_{\mathrm{opt}} = \sqrt[4]{\frac{\eta_\phi^2 - \|\Pi e_\phi\|^2}{\eta^2 - \|\Pi e\|^2}}. \tag{67}$$

Finally, by computing the interval length for the optimum value of α, we attain

$$f(\alpha_{\mathrm{opt}}) = \sqrt{(\eta^2 - \|\Pi e\|^2)(\eta_\phi^2 - \|\Pi e_\phi\|^2)} \leq \sqrt{\eta^2 \eta_\phi^2} = \eta\eta_\phi \tag{68}$$

which is exactly the half of the size of the interval in eq. (33).

30

A.2 Independence of the homogenised conductivity field

We prove that

$$\eta_{\text{Upp}}^{\text{QoI}} + q(\bar{u}^h), \tag{69}$$

the upper bound for $q(u)$ is independent of the conductivity field. The proof of the lower bound is similar. Expanding and rearranging the terms,

$$R(\bar{\phi}^h) + q(\bar{u}^h) + \underbrace{\frac{1}{2}\sqrt{(\eta^2 - \|\Pi e\|^2)(\eta_\phi^2 - \|\Pi e_\phi\|^2)}}_{=:C} +$$

$$+\frac{1}{2}E\left[\int_\Omega k^{-1}(\hat{\boldsymbol{q}}^h + k\nabla\bar{u}^h)(\hat{\boldsymbol{q}}_\phi^h + k\nabla\bar{\phi}^h)\right] + \frac{1}{2}a(\Pi e, \Pi e_\phi) =$$

$$= l(\bar{\phi}^h) - a(\bar{u}^h, \bar{\phi}^h) + q(\bar{u}^h) + C+$$

$$\frac{1}{2}\int_\Omega (\hat{\boldsymbol{q}}^h\nabla\bar{\phi}^h + E\left[k^{-1}\right]\hat{\boldsymbol{q}}^h\hat{\boldsymbol{q}}_\phi^h + \hat{\boldsymbol{q}}_\phi^h\nabla\bar{u}^h + E\left[k\right]\nabla\bar{u}^h\nabla\bar{\phi}^h)\,d\Omega+$$

$$+\frac{1}{2}[a(\Pi u, \Pi\phi) - a(\Pi u, \bar{\phi}^h) - a(\bar{u}^h, \Pi\phi) + a(\bar{u}^h, \bar{\phi}^h)]$$

Grouping in C' the terms that do not depend on $\bar{k}$,

$$C' = C + \frac{1}{2}a(\Pi u, \Pi\phi) + \frac{1}{2}\int_\Omega E\left[k^{-1}\right]\hat{\boldsymbol{q}}^h\hat{\boldsymbol{q}}_\phi^h\,d\Omega, \tag{70}$$

and noting that,

$$a(\Pi u, \bar{\phi}^h) = -\int_\Omega \hat{\boldsymbol{q}}^h\nabla\bar{\phi}^h = l(\bar{\phi}^h)$$

$$a(\bar{u}^h, \bar{\phi}^h) = \int_\Omega E\left[k\right]\nabla\bar{u}^h\nabla\bar{\phi}^h\,d\Omega$$

we attain,

$$\eta_{\text{Upp}}^{\text{QoI}} + q(\bar{u}^h) = C' + q(\bar{u}^h) + \frac{1}{2}\int_\Omega \hat{\boldsymbol{q}}_\phi^h\nabla\bar{u}^h\,d\Omega - \frac{1}{2}a(\bar{u}^h, \Pi\phi) \tag{71}$$

The proof is concluded by considering the upper bound of a temperature field $\bar{v}^h$, resulting from another conductivity field, although using the same discretisation. Subtracting both quantities

$$\eta_{\text{Upp}}^{\text{QoI}} - \eta_{\text{Upp}}^{\text{QoI}\,\prime} + q(\bar{u}^h - \bar{v}^h) = q(\bar{u}^h - \bar{v}^h) + \frac{1}{2}\int_\Omega \hat{\boldsymbol{q}}_\phi^h\nabla(\bar{u}^h - \bar{v}^h)\,d\Omega - \frac{1}{2}a(\bar{u}^h - \bar{v}^h, \Pi\phi) = 0 \tag{72}$$

since $\bar{u}^h - \bar{v}^h \in \mathcal{U}_0^h$ and

$$a(v, \Pi\phi) = -\int_\Omega \hat{\boldsymbol{q}}_\phi^h\nabla v = q(v) \quad \forall v \in \mathcal{U}_0^h. \tag{73}$$

A.3 The effect of the contrast of the material properties

We show under certain assumptions that as the contrast between the conductivities of the constituents is increased, the intervals defined by the error estimates also grow. More precisely, we will show that η grows with the increase in the contrast and we will assume that p_i the probability of being inside the constituent i is the same for every point of the domain, hence $E[k]$ and $E[k^{-1}]$ are not a function of $\boldsymbol{x}$.

We start by decomposing the problem in eq. (2) in the following two problems,

For all $v \in \mathcal{U}_0$, find $\bar{u}_N \in \mathcal{U}_0$

$$\bar{a}(\bar{u}_N, v) = l(v). \tag{74}$$

and

For all $v \in \mathcal{U}_0$, find $\bar{u}_D \in \mathcal{U}$

$$\bar{a}(\bar{u}_D, v) = 0. \tag{75}$$

We note that for $\bar{k}$ constant over the domain:

- $\bar{u}_N + \bar{u}_D$ is a solution to eq. (2). Hence, $\bar{u}_N + \bar{u}_D$ is KA and SA.

- $\bar{u}_D$ and $\nabla \bar{u}_D$ are independent of the value of $\bar{k}$.

- $\bar{q} := -\bar{k} \nabla \bar{u}_N$ is independent of the value of $\bar{k}$.

- $a(\bar{u}_D, \bar{u}_N) = 0$.

We will denote the solutions of those two problems for $\bar{k} = E[k]$ by $\bar{u}_N$ and $\bar{u}_D$ respectively. From the observations, the solutions for $\bar{k} = 1/E[k^{-1}]$ can be expressed as $\bar{u}'_D := \bar{u}_D$ and $\bar{u}'_D := E[k]E[k^{-1}]\bar{u}_N$.

Next, we calculate η^2 with $\hat{\boldsymbol{q}}^h = -1/E[k^{-1}]\nabla(\bar{u}'_D + \bar{u}'_N)$ and with $\bar{u}^h = \bar{u}_D + \bar{u}_N$ and obtain,

$$\eta^2 = \left(E[k] - \frac{1}{E[k^{-1}]} \right) \int_\Omega \nabla \bar{u}_D \cdot \nabla \bar{u}_D \, d\Omega + \left(E[k^{-1}] - \frac{1}{E[k]} \right) \int_\Omega \bar{\boldsymbol{q}} \cdot \bar{\boldsymbol{q}} \, d\Omega. \tag{76}$$

We remark that in eq. (76), only the expression inside the parenthesis depends on the contrast between the particles. The integrals are independent of $\bar{k}$ and hence independent of the conductivity of the constituents. Expressing $E[k]$ and $E[k^{-1}]$ as,

$$E[k] = \sum_{i=1}^N p_i k_i \tag{77}$$

$$E[k^{-1}] = \sum_{i=1}^N \frac{p_i}{k_i} \quad \text{where} \quad \sum_{i=1}^N p_i = 1 \tag{78}$$

where k_i is the conductivity and p_i probability of being inside constituent i, we observe that $E[k]$ is the weighted arithmetic mean of the conductivities, while $1/E[k^{-1}]$ is the weighted harmonic mean of the conductivities. Hence, the two expressions inside parenthesis in eq. (76) are non-negative due to the inequality between the arithmetic and harmonic mean. In addition, these expressions are equal to 0 only and only if $k_1 = k_2 = ... = k_N$. Furthermore, as the contrast between conductivities increases, the quantities increase without bound.

A.4 Statically admissible FEM approximation

Numerical solutions of the homogenised problem (eq. (9)) are sought by means of a hybrid finite element formulation where the fluxes are independently approximated in each element,

$$\hat{\boldsymbol{q}}_e^h = \boldsymbol{Q}_e^h \boldsymbol{w}_e + \hat{\boldsymbol{q}}_{e0}^h \boldsymbol{q}_{h0}^e, \tag{79}$$

with $\boldsymbol{Q}_e^h$ defining an approximation basis such that $\nabla \cdot \boldsymbol{Q}_e^h = 0$, $\boldsymbol{w}_e$ representing the corresponding weights, and $\hat{\boldsymbol{q}}_{e0}^h$ being an arbitrary particular solution verifying $\nabla \cdot \hat{\boldsymbol{q}}_{e0}^h(\boldsymbol{x}) = f(\boldsymbol{x})$. This implies a broken space for the approximation of the fluxes, which locally verifies equilibrium inside the elements, but fails to do so at the boundaries.

To impose equilibrium at the interfaces, so that the resulting flux field $\hat{\boldsymbol{q}}^h$ is in $\mathcal{S}$, the formulation also considers an approximation for the temperatures on the boundaries (external or inter elemental) that do not belong to Γ_D:

$$u_{\Gamma k}^h = \boldsymbol{U}_k^h \hat{\boldsymbol{u}}_k. \tag{80}$$

This implies the consideration of an additional functional, corresponding to the product of the normal flux with the temperatures on the boundaries:

$$b_\Gamma(\boldsymbol{q}, u_\Gamma) = \int_\Gamma (\boldsymbol{q}(\boldsymbol{x}) \cdot \boldsymbol{n}(\boldsymbol{x})) \, u_\Gamma(\boldsymbol{x}) \, d\Gamma.$$

The corresponding hybrid finite element formulation can then be written as

$$\begin{aligned} \boldsymbol{F}\boldsymbol{w} + \boldsymbol{D}^T \hat{\boldsymbol{u}} &= \boldsymbol{x} \\ \boldsymbol{D}\boldsymbol{w} &= \boldsymbol{y} \end{aligned} \tag{81}$$

where the global matrices of flexibility, $\boldsymbol{F}$, and boundary equilibrium, $\boldsymbol{D}$, are obtained by assembling the corresponding elementary contributions, $\boldsymbol{F}_e = b(\boldsymbol{Q}_e^h, \boldsymbol{Q}_e^h)$ and $\boldsymbol{D}_{ek} = b_\Gamma(\boldsymbol{Q}_e^h, \boldsymbol{U}_k^h)$ with

$$b(\boldsymbol{q}, \boldsymbol{p}) = \int_\Omega \hat{k}(\boldsymbol{x}) \boldsymbol{q}(\boldsymbol{x}) \cdot \boldsymbol{p}(\boldsymbol{x}) \, d\Omega. \tag{82}$$

The right hand side terms are computed for each element or interface as

$$\boldsymbol{x} = b(\boldsymbol{q}_{h0}^e, \boldsymbol{Q}_h^e) + b_{\Gamma_D}(\boldsymbol{Q}_h^e, h) \quad \text{and} \quad \boldsymbol{y} = b_{\Gamma_D}(g, \boldsymbol{U}_h). \tag{83}$$

We consider simplicial finite elements (triangles and tetrahedra) with straight/planar interfaces. In this case when $\boldsymbol{Q}_e^h$ is obtained from a complete polynomial basis of degree d_Q the corresponding normal fluxes are polynomial functions of the same degree. The temperatures on the interfaces are independently approximated on each edge of face using complete polynomial basis of degree d_{u_Γ}.

If f and g are polynomial functions of degree d_f and d_g, equilibrium is strictly verified by the finite element solution when $d_Q \geq d_f + 1$, $d_Q \geq d_g$ and $d_Q = d_{u_\Gamma}$. The type of function considered for the imposed temperature, h, has no influence on equilibrium.

Unlike what happens in elasticity, where matrix $\boldsymbol{D}$ may be rank deficient, leading to spurious kinematic modes in the solution and to the existence of inadmissible loadings, for potential problems the resulting finite element model is always stable, leading to unique solutions in terms of fluxes and of boundary temperatures. The only problematic situation is the case of a domain where only Neumann boundary conditions are imposed. In this case the boundary temperatures are not uniquely determined and the imposed boundary fluxes have to balance the internal heat sources.

A.5 Derivation of a deterministic bound for the second moment

The proof is done in 2 parts. In the first part, we find an upper bound for m_2 that only depend on computable quantities. Secondly, we show that the computation of this bound is deterministic. Firstly, through algebraic manipulations, we can show that

$$m_2 - q(\bar{u}^h)^2 = 2q(e)q(\bar{u}^h) + E\left[q_\theta(e)^2\right] \tag{84}$$

The first term can be upper bounded by

$$2q(e)q(\bar{u}^h) \leq 2\Delta q(\bar{u}^h) \tag{85}$$

where Δ is one of the upper estimates from eqs. (33) and (37) if $q(\bar{u}^h)$ is positive, and a lower estimate otherwise. Regarding the second term, it is easy to prove that

$$q_\theta(e) = a_\theta(e, e_\phi) + R_\theta(\phi^h) \tag{86}$$

By squaring both sides and taking the expectation, we obtain

$$E\left[q_\theta(e)^2\right] = E\left[a_\theta(e, e_\phi)^2 + R_\theta(\bar{\phi}^h)^2 + 2a_\theta(e, e_\phi)R_\theta(\bar{\phi}^h)\right] \tag{87}$$

Firstly, the term $E\left[a_\theta(e, e_\phi)^2\right]$ is bounded. By applying the Cauchy-Schwarz inequality

$$a_\theta(e, e_\phi) \leq \|e\|_\theta \|e_\phi\|_\theta \tag{88}$$

followed by the Prager-Synge hypercircle theorem, we obtain

$$\|e\|_\theta \|e_\phi\|_\theta \leq \|\hat{\boldsymbol{q}} + k\nabla\bar{u}^h\|_{\theta, k^{-1}} \|\hat{\boldsymbol{q}}_\phi + k\nabla\bar{\phi}^h\|_{\theta, k^{-1}} \tag{89}$$

This allows us to conclude that

$$E\left[a_\theta(e, e_\phi)^2\right] \leq \underbrace{E\left[\|\hat{\boldsymbol{q}} + k\nabla\bar{u}^h\|_{\theta, k^{-1}}^2 \|\hat{\boldsymbol{q}}_\phi + k\nabla\bar{\phi}^h\|_{\theta, k^{-1}}^2\right]}_{=:\gamma^2} \tag{90}$$

where

$$\|v\|_{\theta, k^{-1}} := \sqrt{\int_\Omega k(\boldsymbol{x}, \theta)^{-1} v(\boldsymbol{x})^2 \, d\Omega}. \tag{91}$$

Next, we bound $E\left[R_\theta(\bar{\phi}^h)^2\right]$. By expanding it, we obtain,

$$E\left[R_\theta(\bar{\phi}^h)^2\right] = l(\bar{\phi}^h)^2 - 2l(\bar{\phi}^h)a(\bar{u}^h, \bar{\phi}^h) + \underbrace{E\left[a_\theta(\bar{u}^h, \bar{\phi}^h)^2\right]}_{=:\beta^2}$$

Finally, we have to bound the cross term in equation eq. (87)

$$\begin{aligned}
E\left[2a_\theta(e, e_\phi)R_\theta(\bar{\phi}^h)\right] &= 2l(\bar{\phi}^h)a(e, e_\phi) - 2E\left[a_\theta(e, e_\phi)a_\theta(\bar{u}^h, \bar{\phi}^h)\right] \\
&\leq 2\Delta' l(\bar{\phi}^h) - 2E\left[a_\theta(e, e_\phi)a_\theta(\bar{u}^h, \bar{\phi}^h)\right] \\
&\leq 2\Delta' l(\bar{\phi}^h) + 2\sqrt{E\left[a_\theta(e, e_\phi)^2\right]}\sqrt{E\left[a_\theta(\bar{u}^h, \bar{\phi}^h)^2\right]} \\
&\leq 2\Delta' l(\bar{\phi}^h) + 2\gamma\beta
\end{aligned}$$

where again, Δ' is a is one of the upper estimates from eqs. (33) and (37) if $l(\bar{\phi}^h)$ is positive, and a lower estimate otherwise. Combining those results, we obtain that

$$m_2 - q(\bar{u}^h)^2 \leq (\gamma + \beta)^2 + 2[\Delta q(\bar{u}^h) + \Delta' l(\bar{\phi}^h)] + l(\bar{\phi}^h)[R(\bar{\phi}^h) - a(\bar{u}^h, \bar{\phi}^h)] \tag{92}$$

Now, we have to show that β and γ are deterministic quantities. We start by expanding β^2

$$\beta^2 = E\left[a_\theta(\bar{u}^h, \bar{\phi}^h)^2\right] = E\left[\int_\Omega k\nabla\bar{u}^h \cdot \nabla\bar{\phi}^h \, d\Omega \int_\Omega k\nabla\bar{u}^h \cdot \nabla\bar{\phi}^h \, d\Omega\right] \tag{93}$$

By combining the two domain integrals into one and switching the order of the integrals (the prime indicates whether a term belongs to the first or the second domain integral),

$$\beta^2 = E\left[\int_\Omega \int_{\Omega'} kk'(\nabla\bar{u}^h \cdot \nabla\bar{\phi}^h)(\nabla u'^h \cdot \nabla\phi'^h) \, d\Omega \, d\Omega\right]$$
$$= \int_\Omega \int_{\Omega'} E\left[kk'\right](\nabla\bar{u}^h \cdot \nabla\bar{\phi}^h)(\nabla u'^h \cdot \nabla\phi'^h) d\Omega \, d\Omega$$

which is a deterministic function. The spatial function $E[kk']$ is actually the covariance of the conductivity plus a constant,

$$Cov(k(\boldsymbol{x}), k(\boldsymbol{x}')) = E[k(\boldsymbol{x})k(\boldsymbol{x}')] - E[k(\boldsymbol{x})]E[k(\boldsymbol{x}')] \tag{94}$$

Proceeding in an analogue manner, we can show that γ is also a deterministic quantity,

$$\gamma^2 = \int_\Omega \int_{\Omega'} \{E[k^{-1}k'^{-1}](\hat{\boldsymbol{q}} \cdot \hat{\boldsymbol{q}})(\hat{\boldsymbol{q}}'_\phi \cdot \hat{\boldsymbol{q}}'_\phi) + E[kk'](\nabla\bar{u}^h \cdot \nabla\bar{u}^h)(\nabla\phi'^h \cdot \nabla\phi'^h) +$$
$$E[k^{-1}k'](\hat{\boldsymbol{q}} \cdot \hat{\boldsymbol{q}})(\nabla\phi'^h \cdot \nabla\phi'^h) + E[kk'^{-1}](\nabla\bar{u}^h \cdot \nabla\bar{u}^h)(\hat{\boldsymbol{q}}'_\phi \cdot \hat{\boldsymbol{q}}'_\phi)\} \, d\Omega \, d\Omega$$
$$+2\int_\Omega \hat{\boldsymbol{q}}_\phi \cdot \nabla\bar{\phi}^h \, d\Omega \left[\int_\Omega \{E[k^{-1}](\hat{\boldsymbol{q}} \cdot \hat{\boldsymbol{q}}) + E[k](\nabla\bar{u}^h \cdot \nabla\bar{u}^h)\} \, d\Omega\right]$$
$$+2\int_\Omega \hat{\boldsymbol{q}} \cdot \nabla\bar{u}^h \, d\Omega \left[\int_\Omega \{E[k^{-1}](\hat{\boldsymbol{q}}_\phi \cdot \hat{\boldsymbol{q}}_\phi) + E[k](\nabla\phi^h \cdot \nabla\phi^h)\} \, d\Omega\right]$$
$$+4\int_\Omega \hat{\boldsymbol{q}} \cdot \nabla\bar{u}^h \, d\Omega \int_\Omega \hat{\boldsymbol{q}}_\phi \cdot \nabla\bar{\phi}^h \, d\Omega$$